



Document ID	Version	Status	Reg no	Page
1415878	1.0	Godkänt		1 (43)
Author			Date	
Lennart Börjesson, Mattias Åkesson, Jan Hernel			2013-11-25	

3.2 Analysis of risks and consequences of uneven wetting in a dry deposition hole

Lennart Börjesson
Mattias Åkesson
Clay Technology AB

Jan Hernelind
5T Engineering AB

Table of Contents

	Page
1. Introduction	2
2. Inflow scenarios	2
2.1 General	2
2.2 Matrix flow in the rock	2
2.3 Free water inflow	2
2.4 Water distribution in a pellet filling	5
3. Water transport in a pellet filled slot at very low inflow rates, modelled as a diffusion process with free access of water	8
3.1 Moisture diffusivity in pellets-filled slots	8
3.2 Water-uptake calculation	13
4. FEM modelling of the wetting and homogenisation of the buffer at heterogeneous water inflow distribution	17
4.1 General	17
4.2 Finite element code Abaqus	17
4.3 Element mesh	17
4.4 Material models	18
4.5 Modelling strategy	21
4.6 Modelling results – constant inflow rate	22
4.7 Modelling results – constant water pressure	36
5. Risks and consequences	42
References	46

1. Introduction

The deposition holes and tunnels in the Forsmark repository are foreseen to be very dry with none or a single inflow point in most of the deposition holes. The question of how a low inflow rate in single points in a deposition hole affects the wetting and homogenisation of the buffer has been raised and is analysed in this PM.

In general uneven wetting is not expected to yield any homogenisation problems since the swelling and homogenisation processes are not very stress path dependant. If the buffer starts swelling at one point the influence on the unswelled parts are not very strong and possible displacements of the buffer is small due to the confinement of the buffer inside the rock surface. The displacements that take place are to a large part expected to be reversed by the late swelling of the other parts of the buffer. However, research concerning this question is on-going.

This report includes a theoretical study of the moisture transport in dry pellet filling and the consequences for the wetting. It also includes simulations of some critical cases with uneven wetting.

2. Inflow scenarios

2.1 General

The expected inflow distribution in the deposition holes in the Forsmark repository has been analysed and reported (Svensson and Follin 2010, Joyce et al. 2013). According to Joyce et al. (2013) the total number of deposition holes with an inflow rate higher than 10^{-5} L/min is about 1350 out of 6916 holes. The majority of the deposition holes thus has a very low inflow rate.

The water inflow from a single fracture or channel in the rock into a deposition hole is only of interest if the water supply from the matrix is lower than from the fracture. The hydraulic conductivity of the rock matrix in Forsmark is thus an important input parameter to the analysis. It has been measured for a large number of rock core samples by Vilks (2007). Almost all tests showed a hydraulic conductivity of the matrix of between $2 \cdot 10^{-12}$ m/s and $1 \cdot 10^{-13}$ m/s. Only a few tests at high external pressure resulted in a hydraulic conductivity below $1 \cdot 10^{-13}$ m/s.

2.2 Matrix flow in the rock

The distribution of inflow between matrix flow and fracture flow at low inflow rate is not clear. It may be a matter of definition but for the wetting of the buffer it is interesting to study the effect of having a low inflow rate into a point of the deposition hole without considering the matrix flow. In order to get the perspective, modelled time to full water saturation in the case of only matrix flow and a low rock matrix hydraulic conductivity is in the order of 1 500 years at $K_{\text{rock}}=10^{-13}$ m/s and 15 000 years at $K_{\text{rock}}=10^{-14}$ m/s (Åkesson et al. 2010a).

2.3 Free water inflow

A number of time limits can be set for bounding the time it may take to fill up the pellet filling with water and for saturating the buffer blocks. The available pore space is defined by the density and degree of saturation of the different bentonite parts and the geometry of the deposition hole, the canister and the bentonite blocks and rings. Table 2-1 shows the bentonite properties (taken from the modelling of the CRT in (Åkesson et al. 2010a)) and Figure 2-1 shows the geometry used for the calculations. The geometry is not totally identical to the geometry shown in the production report of the buffer (SKB 2010), but the difference is not significant for the results.

Table 2-1. Basic properties of the bentonite parts.

Section	Density (kg/m ³)	Water ratio	Dry density (kg/m ³)	Void ratio	Degr. of saturation
Solid block	1991	0.172	1699	0.636	0.751
Ring shaped block	2087	0.171	1782	0.560	0.849
Pellets (17%)	1162	0.186	993	1.78	0.29

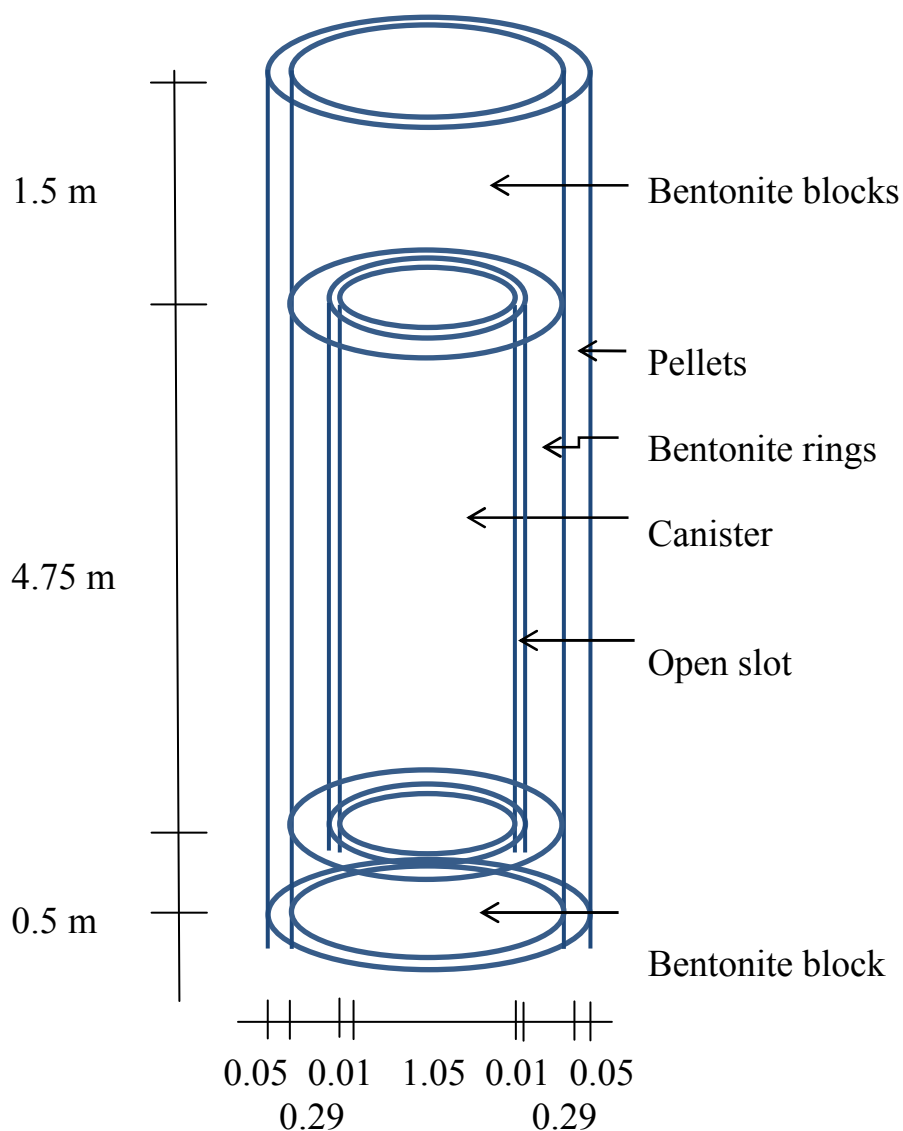


Figure 2-1. Geometry of the deposition hole with the canister and the bentonite.

Volume calculations

Pellets

Volume of pellets:

$$V_p = H \cdot D \cdot \pi \cdot \Delta r = 6.75 \cdot 1.7 \pi \cdot 0.05 = 1.80 \text{ m}^3$$

where H=height, D=diameter, Δr =aperture of pellet filled slot

Available pore space in pellets:

$$V_{pp} = n \cdot V_p = V_p \cdot e / (1 + e) = 1.15 \text{ m}^3$$

where n=porosity, e=void ratio

Empty pore space:

$$V_{ppe} = V_{pp} \cdot (1 - S_r) = 0.817 \text{ m}^3$$

Solid blocks

Volume of blocks:

$$V_b = H \cdot \pi \cdot D^2 / 4 = 2.0 \cdot \pi \cdot 1.65^2 / 4 = 4.28 \text{ m}^3$$

where H=height, D=diameter, Δr =aperture of pellet filled slot

Available pore space in blocks:

$$V_{pb} = n \cdot V_b = V_b \cdot e / (1 + e) = 1.66 \text{ m}^3$$

where n=porosity, e=void ratio

Empty pore space:

$$V_{pbe} = V_{pb} \cdot (1 - S_r) = 0.414 \text{ m}^3$$

Rings

Volume of rings:

$$V_p = H \cdot (D_o^2 - D_i^2) \cdot \pi / 4 = 6.75 \cdot (1.65^2 - 1.07^2) \cdot \pi / 4 = 8.36 \text{ m}^3$$

where H=height, D_o =outer diameter, D_i =inner diameter

Available pore space in rings:

$$V_{pr} = n \cdot V_p = V_p \cdot e / (1 + e) = 3.00 \text{ m}^3$$

where n=porosity, e=void ratio

Empty pore space:

$$V_{pre} = V_{pr} \cdot (1 - S_r) = 0.453 \text{ m}^3$$

Inner slot:

Volume of inner slot:

$$V_s = H \cdot D \cdot \pi \cdot \Delta r_s = 4.75 \cdot 1.06 \cdot \pi \cdot 0.01 = 0.158 \text{ m}^3$$

where H =height, D =diameter, Δr_s =aperture of inner slot

Total empty volume is thus

$$V_{te}=1.842 \text{ m}^3 \text{ whereof}$$

$$V_{ppe}= 0.817 \text{ m}^3$$

Inflow 0.0001 L/min yields 35 years to saturate the buffer. See Table 2-2.

Table 2-2. Time to fill all empty space in the pellets filled slot and time to saturate the entire buffer in case of constant water inflow rate.

Inflow (L/min)	Time to fill pellets slot (years)	Modelled time (years)	Time to fill all voids (years)	Modelled time (years)
$1.0 \cdot 10^{-3}$	1.55		3.5	
$1.0 \cdot 10^{-4}$	15.5	$\approx 150/1500$	35	≈ 1500
$1.0 \cdot 10^{-5}$	155		350	
$1.0 \cdot 10^{-6}$	1 550	1500-2000	3 500	
$1.0 \cdot 10^{-7}$	15 500		35 000	

The times calculated refer to the case that the inflow rate is constant irrespective of the water pressure required. In the modelling (se later) the reduced inflow that will be the case if a water pressure is generated in the fracture is taken into account.

2.4 Water distribution in a pellet filling

A critical process for the wetting is how the water is distributed in the pellet filling. The water transport properties in pellet filling are complicated and the water distribution caused by water inflow difficult to predict, not always repeatable and to some extent random. There is also an influence of pellet type, bentonite type and salt concentration. However, there are some patterns observed that can be used to formulate a “model” although very primitive and uncertain. The pellet type to be used in the deposition holes is not finally decided. The model is mainly based on results on the tests made on roller compacted pellets made of MX-80 according to the reference design as described in the production report of the buffer (SKB 2010) but may probably also be used for extruded pellets although it seems as the limits are moved towards higher inflow rates for those pellets. The limits between the different patterns are not clear but a successive transition is assumed.

$$q \geq 0.1 \text{ L/min}$$

At very high inflow rates, the water inflow is faster than the individual pellets can absorb so the free water will fill up the empty pore space and by gravity flow downwards. The deposition hole will be filled like a bathtub.

$$q = 0.01 \text{ L/min}$$

At fairly high inflow rates, the flow is spread equally in all directions and thus fills the slot circularly with the inflow point as centre and with increasing radius with time. There might though be a tendency for upwards movements. When the water reaches a free surface it seems as the continuing flow mainly goes to the surface.

$$q = 0.001 \text{ L/min}$$

At low inflow rates, the flow seems to move upwards in a rather narrow channel. Once it reaches a free surface of the pellet filling the water stays there and continues to flow out on the surface. The reason for the upwards flow is not clear. The phenomenon is empirically observed but it is not yet clear if it fundamentally correct to assume that it always will take place.

$$q=0.0001 \text{ L/min}$$

At very low inflow rates, the inflow pattern seems to go back to something between the pattern at 0.001 L/min and 0.01 L/min. An elliptic pattern seems to be formed with a tendency to move upwards and with the major axis directed vertically.

$$q \leq 0.00001 \text{ L/min}$$

At extremely low inflow rates, the water seems to follow a diffusion like behaviour and spread as concentric circles, similar to that at 0.01 l/min.

The “model” is illustrated in Figure 2-2.

The flow behaviour is important to understand in order to be able to predict how heterogenic the bentonite blocks are wetted at very low inflow rates from single fractures in dry deposition holes. The “model” presented is very uncertain but is judged sufficient for the purposes of the present study.

Since the flow rates of interest at dry rock conditions is below 0.0001 L/min, water uptake from a single point in a deposition hole can be assumed to behave in a diffusion like pattern, the last picture in Figure 2-2, with equal distribution of moisture in all directions.

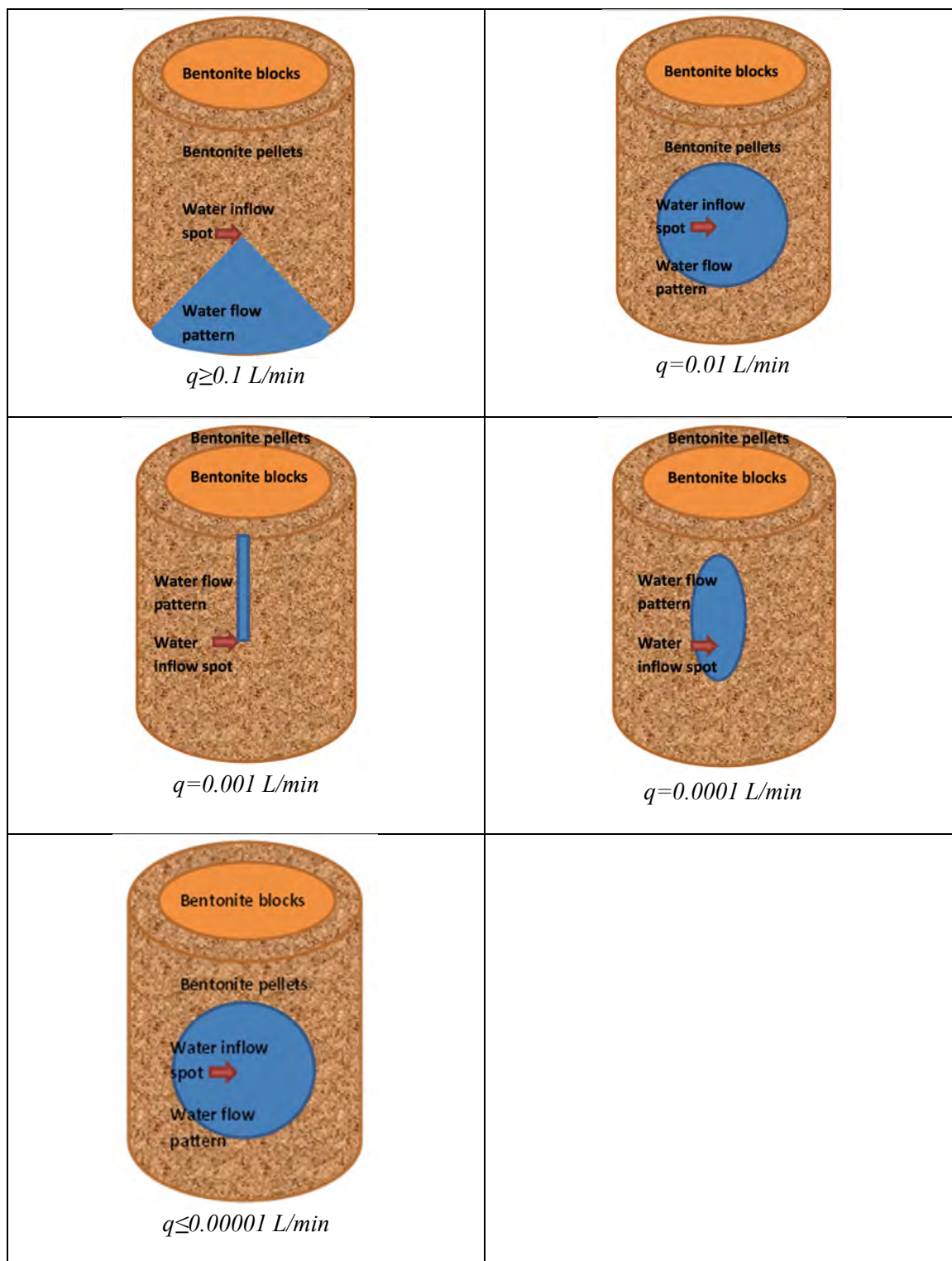


Figure 2-2. Simple “model” of water flow distribution in the pellet filled slot in the deposition holes. The limits between the different patterns are not clear but a successive transition is assumed.

3. Water transport in a pellet filled slot at very low inflow rates, modelled as a diffusion process with free access of water

3.1 Moisture diffusivity in pellets-filled slots

3.1.1 Introduction

The apparently slow water-uptake in bentonite pellets has raised the question whether moisture transfer in pellets may be governed by vapour diffusion. An analysis has therefore been performed with the aim to quantify the moisture transfer flow coefficients for different dry densities and water contents, in general, and for typical pellets conditions, in particular. The results from this analysis are presented in this chapter.

The bentonite is regarded as a system of two phases: water-saturated grains and gas-filled voids, in which the moisture is transferred as liquid or as vapour, respectively. Both these fluxes are described as driven by gradients in water content, and moisture diffusivity values for liquid as well as vapour can be quantified in this way.

An effective diffusivity value is finally estimated for the bentonite as a whole, and for this the phases are assumed to behave as a composite medium arranged either in series or in parallel (Figure 3-1). The relative distribution of these phases is assumed to be equal to the fraction of grains and gas-filled voids, respectively.

It is found that the moisture diffusivity value for the two phases appears to coincide at a moisture content of approximately 20-30%. Below this level the effective diffusivity appears to be limited by liquid transfer whereas the vapour transfer can be limiting above the level.

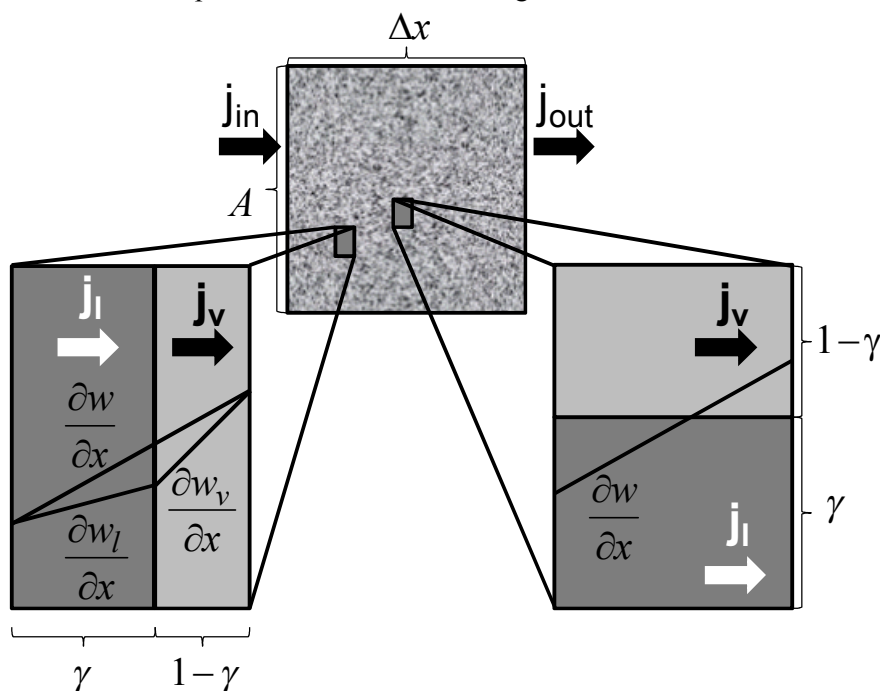


Figure 3-1. Schematic outline of fluxes in and out of elementary volume, and fluxes in liquid and vapour phase arranged in series or in parallel.

3.1.2 Mass flux and mass conservation

The mass flux (j) is given by gradients in water content (w):

$$j = -D' \cdot \frac{\partial w}{\partial x} \quad (3-1)$$

where the unit of the coefficient D' is $\text{kg} \cdot \text{m}^{-1} \cdot \text{s}^{-1}$.

The next step is to consider an elementary volume with section area A and length Δx (see Figure 3-1). The condition of mass conservation implies that the increase of the water mass in the volume equals the difference between the inflow flux (j_{in}) and outflow flux (j_{out}) through the section area. The mass increase is expressed in terms of a time derivative of the water content:

$$A \cdot \Delta x \cdot \rho_d \cdot \frac{\partial w}{\partial t} = A \cdot (j_{in} - j_{out}) \quad (3-2)$$

where ρ_d is the dry density of the bentonite. The right hand side is developed as:

$$A \cdot (j_{in} - j_{out}) = A \cdot \left[j - \left(j + \frac{\partial j}{\partial x} \Delta x \right) \right] = -A \cdot \Delta x \cdot \frac{\partial j}{\partial x} = A \cdot \Delta x \cdot \frac{\partial}{\partial x} \left(D' \cdot \frac{\partial w}{\partial x} \right) \quad (3-3)$$

Both sides are then divided with dry mass of the volume ($A \cdot \Delta x \cdot \rho_d$), which results in Fick's second law:

$$\frac{\partial w}{\partial t} = \frac{\partial}{\partial x} \left(\frac{D'}{\rho_d} \cdot \frac{\partial w}{\partial x} \right) = \frac{\partial}{\partial x} \left(D \cdot \frac{\partial w}{\partial x} \right) \quad (3-4)$$

The moisture diffusivity D is thus obtained by dividing the coefficient D' with the dry density.

3.1.3 Liquid and vapour mass fluxes

The mass flux through vapour diffusion (j_v) is in Code_Bright described as driven by gradients in vapour mass fraction (ω). This gradient can be developed in terms of gradients in water content:

$$j_v = -\rho_g \cdot D^o \cdot \frac{T^{2.3}}{p_g} \cdot \frac{\partial \omega}{\partial x} = -\rho_g \cdot D^o \cdot \frac{T^{2.3}}{p_g} \cdot \frac{d\omega}{dw} \cdot \frac{\partial w}{\partial x} = -D'_v \cdot \frac{\partial w}{\partial x} \quad (3-5)$$

where ρ_g is the gas density, D^o is a diffusion parameter set to $5.9 \cdot 10^{-6} (\text{m}^2 \text{s}^{-1} \text{K}^{-2.3} \text{Pa})$, T is the absolute temperature and p_g is the gas pressure. The negative ratio between the mass flux and the water content gradient in vapour is denoted D'_v . Note that this flux is found in the gas phase, and the factor used normally in unsaturated porous medium, $\tau \cdot n \cdot (1-S)$, is assumed to be equal to unity. The derivative $d\omega/dw$ is developed in Eq. (3-10) below. The moisture diffusivities for vapour transfer can thus be expressed as:

$$D_v = \frac{\rho_g}{\rho_d} \cdot D^o \cdot \frac{T^{2.3}}{p_g} \cdot \frac{d\omega}{dw} \quad (3-6)$$

Mass flux through water-saturated grains (j_l) is given by Darcy's law and gradients in water activity (liquid pressure, p_l), which is equal to the negative gradient in suction (ψ). This can be developed in terms of gradients in water content:

$$j_l = -\rho_w \frac{k}{\mu} \frac{\partial p_l}{\partial x} = \rho_w \frac{K(w)}{\rho_w \cdot g} \frac{d\psi}{dw} \frac{\partial w}{\partial x} = -D_l' \cdot \frac{\partial w}{\partial x} \quad (3-7)$$

where ρ_w is the water density, k is the permeability, μ is the viscosity, and g is gravity. Hydraulic conductivity, K , is described as a function of water content, see Eq. (3-13) below. The negative ratio between the mass flux and the water content gradient in grains is denoted D_l' . The moisture diffusivities for liquid transfer can thus be expressed as:

$$D_l = -\frac{K(w)}{\rho_d \cdot g} \frac{d\psi}{dw} \quad (3-8)$$

3.1.4 Material models and derivatives

The derivative of the vapour mass fraction with respect to water content in Eq. (3-6) can be calculated with the chain rule:

$$\frac{d\omega}{dw} = \frac{d\omega}{dp_v} \frac{dp_v}{d\psi} \frac{d\psi}{dw} \quad (3-9)$$

The relation between the vapour mass fraction and the vapour pressure (p_v) gives the first derivative:

$$\omega \approx \frac{p_v}{p_g} \frac{M_w}{M_a} \Rightarrow \frac{d\omega}{dp_v} \approx \frac{M_w}{p_g M_a} \quad (3-10)$$

where M_w and M_a are the molar masses for water and air, respectively. The relation between the vapour pressure and suction value is given by Kelvin's law and gives the second derivative:

$$p_v = p_v^{sat} \cdot \exp\left[-\frac{\psi(w) \cdot M_w}{\rho_w RT}\right] \Rightarrow \frac{dp_v}{d\psi} = -p_v^{sat} \cdot \frac{M_w}{\rho_w RT} \cdot \exp\left[-\frac{\psi(w) \cdot M_w}{\rho_w RT}\right] \quad (3-11)$$

Where p_v^{sat} is the saturated vapour pressure, and R is the general gas constant. The retention curve gives the third derivative, and also for the liquid transfer diffusivity in Eq. (3-8). The retention curve used here follows the model for MX-80 presented by Dueck (2007):

$$\psi(w) = \exp[a - bw] - \frac{w - w_{in}}{w_{sat} - w_{in}} \cdot \exp[a - bw_{sat}] \quad (MPa) \quad (3-12)$$

The following parameter values are used for a case with initial water content of 10%:
 $a=6.3$ and $b=16$.

Finally, the following relation for the hydraulic conductivity of MX-80 was adopted by Åkesson et al. (2010b) and used for the liquid transfer diffusivity in Eq. (3-8):

$$K(w) = 2.4 \cdot 10^{-13} \cdot \left(\frac{w \cdot \rho_s}{\rho_w}\right)^{5.33} \quad (3-13)$$

3.1.5 Liquid and vapour transfer in series or in parallel

The condition for moisture transfer in series is illustrated in Figure 3-1. Since the liquid and vapour fluxes have to be equal, this implies the following relation between the water content gradients in the gas phase and in the grains:

$$j_v = j_l \Rightarrow -D_v \frac{\partial w_v}{\partial x} = -D_l \frac{\partial w_l}{\partial x} \Rightarrow \frac{\partial w_v}{\partial x} = \frac{D_l}{D_v} \frac{\partial w_l}{\partial x} \quad (3-14)$$

The overall water content gradient is estimated by weighting the gradients in the phases with respect to the volume fractions of the phases, and with the relations of the gradients in the phases according to Eq. (3-14). In this way a relation between the overall gradient and the gradient in the grains is obtained.

$$\frac{\partial w}{\partial x} = \gamma \cdot \frac{\partial w_l}{\partial x} + (1 - \gamma) \cdot \frac{\partial w_v}{\partial x} = \frac{\partial w_l}{\partial x} \left[\gamma + (1 - \gamma) \cdot \frac{D_l}{D_v} \right] \quad (3-15)$$

γ is defined as the ratio between the specific grain volume and the specific total volume $(1 + w \cdot \rho_s / \rho_w) / (1 + w_{\text{sat}} \cdot \rho_s / \rho_w)$. The overall flux is the same as the flux through the grains, and together with Eq. (3-15) this yields an expression for the effective moisture diffusivity:

$$D_l \frac{\partial w_l}{\partial x} = \frac{D_l}{\gamma + (1 - \gamma) \cdot \frac{D_l}{D_v}} \frac{\partial w}{\partial x} = \frac{1}{\frac{\gamma}{D_l} + \frac{1 - \gamma}{D_v}} \frac{\partial w}{\partial x} = D_{\text{ser}} \frac{\partial w}{\partial x} \Rightarrow D_{\text{ser}} = \frac{1}{\frac{\gamma}{D_l} + \frac{1 - \gamma}{D_v}} \quad (3-16)$$

A corresponding effective diffusivity can be evaluated for a parallel arrangement:

$$D_{\text{par}} = \gamma \cdot D_l + (1 - \gamma) \cdot D_v \quad (3-17)$$

3.1.6 Quantification of diffusivity functions

Evaluated diffusivities, in vapour, liquid, series and parallel are shown for two different cases in Figure 3-2, for water contents in the intervals 13 – 25% (corresponding approximately with buffer dry density), and 10 - 64 % (i.e. typical for pellets-filled slots).

In the first case, D_l displays an increasing trend for increasing water contents, whereas D_v , in contrast, displays a decreasing trend. The values coincide at the level of $5 \cdot 10^{-10} \text{ m}^2/\text{s}$ at a water content of approximately 25%. The effective diffusivity for arrangements in series is quite close to the D_l values, whereas the corresponding values for parallel arrangements are significantly higher for the lower water contents. Both effective diffusivity functions can be regarded as in fairly good agreement with empirical data (see Åkesson 2013).

In the second case, the diffusivity functions are basically the same as in the first case for water content levels below 25%. One exception is D_{parallel} which is much higher in the second case. For higher water contents, the D_l displays a maximum of $7 \cdot 10^{-10} \text{ m}^2/\text{s}$ at 30 - 35% and above that decreases down to $2 \cdot 10^{-10} \text{ m}^2/\text{s}$ at 64%. The D_v , in contrast, displays a strong decreasing trend and falls below $1 \cdot 10^{-10} \text{ m}^2/\text{s}$ at water contents above 35%. The effective diffusivity for arrangements in series is closer to the D_v -values, whereas the corresponding values for parallel arrangements are closer to the D_l -values.

Apart from these direct observations, the following comments can be made concerning the presented approach:

- The effective diffusivity of the serial arrangement tends to be governed by the phase with the lowest diffusivity, i.e. the liquid transfer at $w < 25\%$ and the vapour transfer at $w > 25\%$.
- The validity of the evaluated results is limited by the ranges for which the used parameters were adopted. The hydraulic conductivity relation was indented to be used for dry density values corresponding to water contents of 20-64%, although the empirical data in both ends were quite scarce. Similarly, the retention curve was based on experimental data with water contents of 2-35%. This latter function may be extended with swelling pressure data which was adopted for the same range as the hydraulic conductivity. Therefore, the material model appears to be least founded for water contents below 20%, although the high end values of D_1 may also be updated if more hydraulic conductivity data are considered.
- Retention curve was based on a linear pressure build-up, although alternative functions may also be considered.
- The serial arrangement implies no continuity of the phases, whereas the parallel implies a perfect continuity. The possibility that continuities occurs at the low and high end of the water content range may be considered.

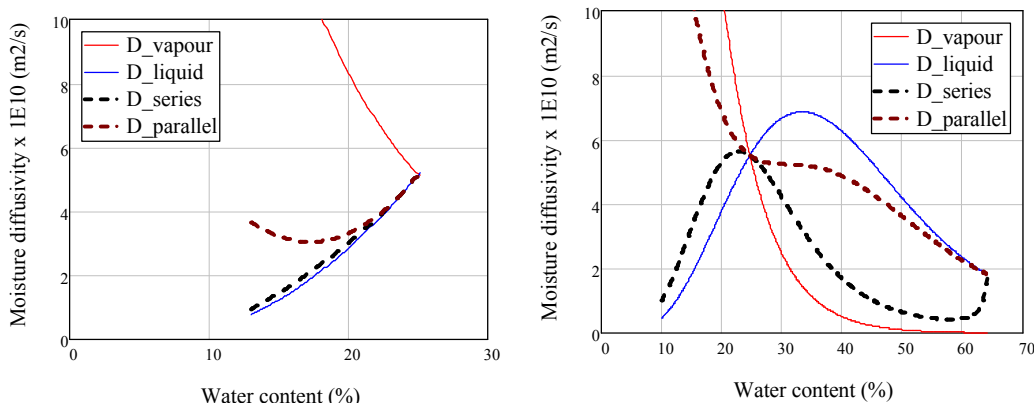


Figure 3-2. Evaluated diffusivity as a function of water content; liquid phase (red thin line); in vapour phase (blue thin line); series (black dotted line) and parallel (brown dotted line). Left graph shows results for water contents between 13-25%. Right graph shows results for 10-64%.

3.2 Water-uptake calculation

3.2.1 Geometrical considerations

A simple case of water-uptake into the pellets-filled slot around the buffer, in which water enters the filling in one point at the mid-height, is illustrated in Figure 3-3. The cylindrical shape is first folded up into a rectangular panel with the water inlet at the centre. This is in turn simplified as a circular panel with the same area as the rectangular panel, again with the inlet as the centre. Finally, this form is identical with a 1D axisymmetric geometry. The height and the circumference of the pellets-filling correspond to an area of 43 m², which in turn corresponds to an outer radius of 3.7 m. The thickness of the filling is 0.05 m. A small inner radius is finally adopted, and this was in this analysis set to 0.01 m, thereby representing a channel with approximately the same dimensions as the voids in the pellets filling.

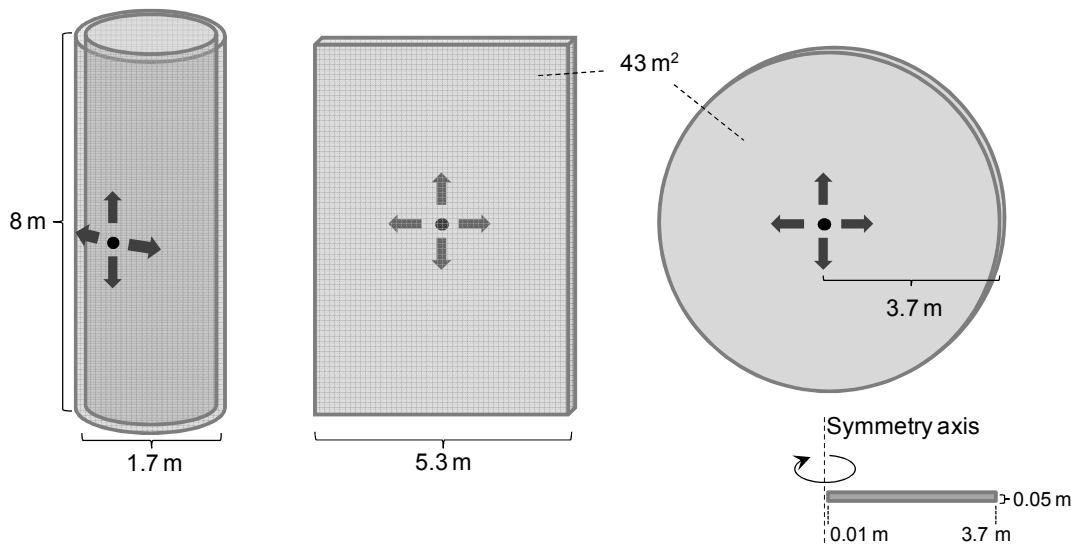


Figure 3-3. Simplification of pellets geometry into a 1D axisymmetric geometry.

3.2.2 Tool for water-uptake calculations

In order to have an efficient and transparent tool for evaluating the water-uptake a MathCad algorithm was prepared, in which the water transport is described by a saturation dependent moisture diffusivity function $D(S)$, and in which the diffusion equation is solved with an explicit finite-difference method.

The 1D radial geometry of the water-uptake tests are discretized in n elements according to Figure 3-4 (left). The index i , with values between 0 and $n-1$, denote the element. The radial width of each element is $\Delta r = (R_{out} - R_{in}) / (n-1)$, except for the inner and outer elements which have half this width. The numerical scheme used to calculate the saturation profile for a point in time, with index j , is illustrated in Figure 3-4 (right). The time step between two successive point in time is denoted Δt .

The diffusion equation for radial diffusion can be developed in the following four terms:

$$\frac{\partial S}{\partial t} = \frac{1}{r} \cdot \frac{\partial}{\partial r} \left(r D \frac{\partial S}{\partial r} \right) = D \frac{\partial^2 S}{\partial r^2} + \frac{D}{r} \cdot \frac{\partial S}{\partial r} + \frac{\partial D}{\partial r} \cdot \frac{\partial S}{\partial r} \quad (3-18)$$

These terms with partial derivatives are estimated with the following corresponding finite differences:

$$\left\{ \begin{array}{l} \frac{\partial S}{\partial t} \approx \frac{S_{j,i} - S_{j-1,i}}{\Delta t} \\ D \frac{\partial^2 S}{\partial r^2} \approx D(S_{j-1,i}) \cdot \frac{S_{j-1,i+1} - 2S_{j-1,i} + S_{j-1,i-1}}{\Delta r^2} \\ \frac{D}{r} \cdot \frac{\partial S}{\partial r} \approx \frac{D(S_{j-1,i})}{R_{in} + i \cdot \Delta r} \cdot \frac{S_{j-1,i+1} - S_{j-1,i-1}}{2 \cdot \Delta r} \\ \frac{\partial D}{\partial r} \cdot \frac{\partial S}{\partial r} \approx \frac{D(S_{j-1,i+1}) - D(S_{j-1,i-1})}{2 \cdot \Delta r} \cdot \frac{S_{j-1,i+1} - S_{j-1,i-1}}{2 \cdot \Delta r} \end{array} \right. \quad (3-19)$$

Note that the radius of element i is expressed as $R_{in} + i \cdot \Delta r$. For convenience, the following constant is defined:

$$R = \frac{\Delta t}{\Delta r^2} \quad (3-20)$$

Based on Equations (3-18) - (3-20), the following expressions can be derived for the saturation degree in all elements, except for the inner and outer elements:

$$\begin{aligned} S_{j,i} = & S_{j-1,i} + R \cdot D(S_{j-1,i}) \cdot [S_{j-1,i+1} - 2S_{j-1,i} + S_{j-1,i-1}] \\ & + \frac{\Delta t}{2\Delta r} \frac{D(S_{j-1,i})}{R_{in} + i \cdot \Delta r} \cdot [S_{j-1,i+1} - S_{j-1,i-1}] \\ & + \frac{R}{4} [D(S_{j-1,i+1}) - D(S_{j-1,i-1})] \cdot [S_{j-1,i+1} - S_{j-1,i-1}] \end{aligned} \quad (3-21)$$

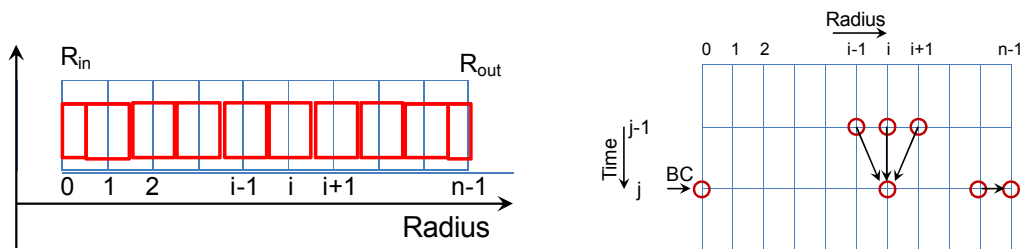


Figure 3-4. Discretization of geometry in n elements with index i , shown as red boxes (left). Numerical scheme used to update the saturation profile (right). Points in time are denoted with index j .

The saturation degree of the outer element is the same as for the adjacent element ($S_{j,n-1} = S_{j,n-2}$), and for the inner element this is given as a boundary condition, which is full saturation ($S_{j,0} = 1$).

The following parameters and geometries were defined for the current problem:

- Inner radius: 0.01 m.

- Outer radius 3.7 m.
- Thickness: 0.05 m.
- Porosity: 0.64.
- Initial saturation: 0.156; based on a water content of 10%.

The discretization in time and space was adjusted for each specific calculation.

3.2.3 Time-scale for water-uptake in pellets-filled slot

The water-uptake in the outlined geometry was modelled for two different moisture diffusivity functions.

In the first case a constant value of $2 \cdot 10^{-10} \text{ m}^2/\text{s}$ was used. This value was chosen since it represents an approximate mean value of the evaluated diffusivity relation for a serial arrangement (see Figure 3-2). The geometry was discretized in 50 elements, and the calculation was performed for the time span of 25 kyears, which was discretized in 60,000 time steps. The time until a saturation degree of 0.99 was reached in the last element was found to be 22 kyears. Results are shown in the left graphs in Figure 3-5.

It can be mentioned that an independent analytical solution for this problem was obtained from Carslaw and Jaeger (1959). This calculation resulted in a slightly slower hydration, and the time to reach a saturation degree of 0.99 at the outer boundary was 25 kyears. This difference may possibly be due to the rough mesh of the numerical solution. Even if the geometry was divided in 50 elements, these elements may still be too large in comparison to the inner radius. The accuracy of the method can nevertheless be considered as sufficiently good at this stage.

In the second case, the following diffusivity function was adopted in order to mimic the evaluated diffusivity relation for a serial arrangement (see Figure 3-6):

$$D_f(w) = \left[0.4 + 64(w - 0.09) \cdot \exp\left[-28 \cdot (w - 0.09)^2\right] \right] \cdot 10^{-10} \quad (\text{m}^2 / \text{s}) \quad (3-22)$$

The geometry was discretized in 30 elements, and the calculation was performed for the time span of 100 kyears, which was discretized in 250,000 time steps. The time until a saturation degree of 0.99 was reached in the last element was found to be 91 kyears. Results are shown in the right graphs in Figure 3-5.

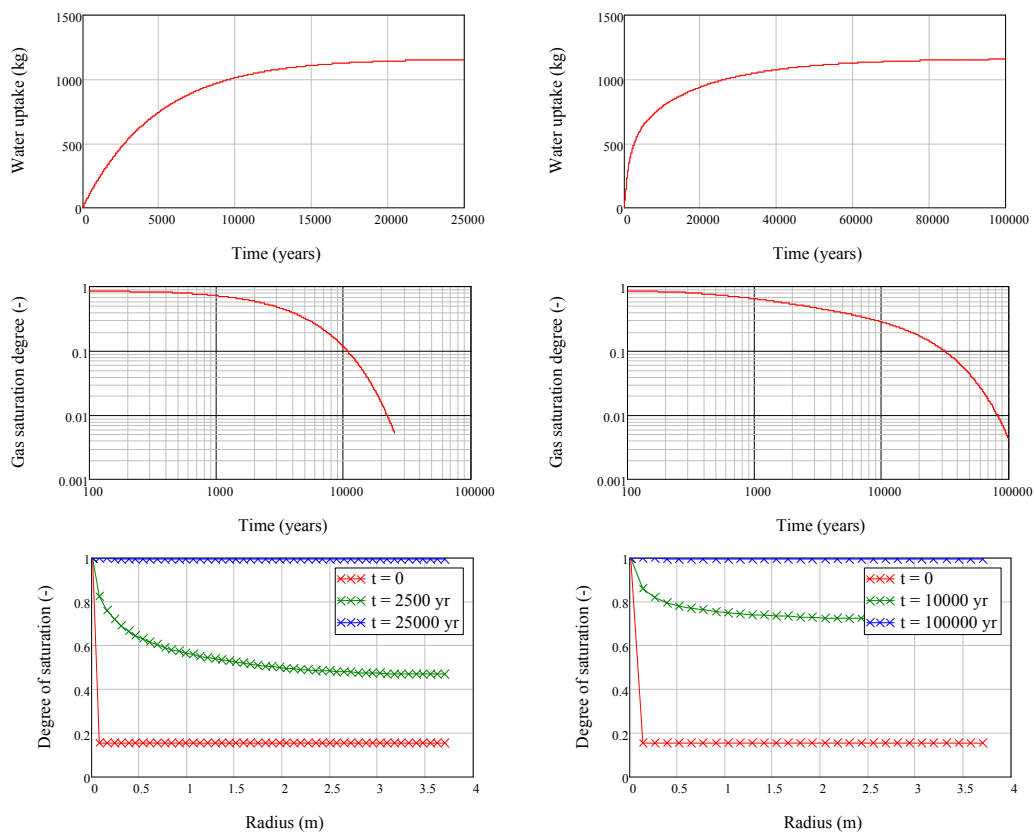


Figure 3-5. Model results for a case with constant diffusivity of $2 \cdot 10^{-10} \text{ m}^2/\text{s}$ (left) and with a water content dependence according to Eq. (3-22) (right): cumulative water uptake (upper), gas saturation ($1-S$) in the outer element (middle) and saturation profiles (lower).

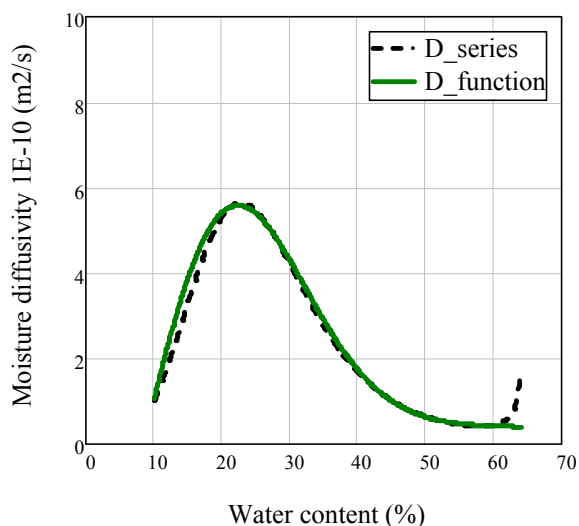


Figure 3-6. Adopted diffusivity function (green solid) mimicking evaluated diffusivity for phases in series (black dotted line).

4. FEM modelling of the wetting and homogenisation of the buffer at heterogeneous water inflow distribution

4.1 General

In order to study the wetting process and the subsequent homogenisation at heterogeneous inflow distribution, a case with one inflow point has been modelled assuming constant water inflow rate.

In a first attempt, a 3D model of a deposition hole with bentonite blocks, rings and pellets and a canister was analysed with a number of calculations using the finite element code Abaqus and a completely coupled THM processes. These calculations were not successful since convergent solutions could not be reached. In order to try to simplify the calculation all nodes were locked so that the mechanical swelling and homogenisation were disregarded. Also these calculations were problematic but in the end successful. Then the pellet filled slot alone was studied and a number of calculations with different inflow rates were successful.

Finally some simulations with another boundary condition of the water inflow were performed.

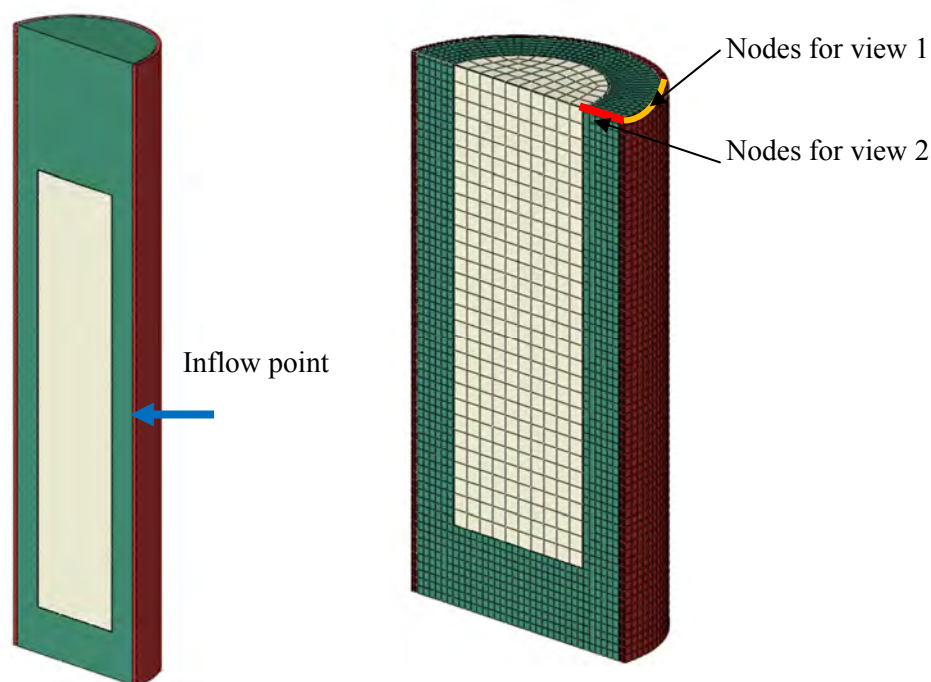
4.2 Finite element code Abaqus

The code Abaqus has been described in previous reports and will not be further described here. See e.g. Åkesson et al. (2010a).

4.3 Element mesh

The dimensions of the different parts of the modelled system are shown in Figure 2-1. The one cm slot between the canister and the bentonite rings are also included.

The geometry and the element mesh are shown in Figure 4-1 together with some result points.



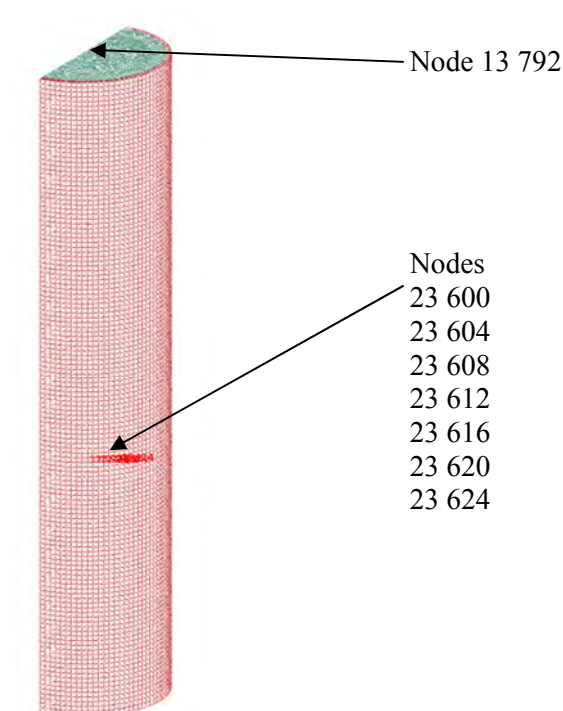


Figure 4-1. Element geometry and half of the element mesh (upper). The vertical surface is a symmetry plane. Some nodes that are used to plot results are also shown.

4.4 Material models

The basic properties of the three bentonite parts are shown in Table 2-1. The material models of the bentonite blocks and rings are identical to the models used in Åkesson et al. (2010a) for modelling the Canister Retrieval Test, CRT, with Abaqus (Section 5.13.2). The model of the bentonite pellets differs however, since the pellets filled slot was water filled in CRT but is dry in the present model (no artificial water filling will be done according to the reference concept).

A hydro-mechanical model of a pellets filled slot that can be used in finite element calculations together with the established models of highly compacted bentonite has not been formulated before and there is a need for further tests and model development. As seen in Figure 2-2, the behaviour is very different depending on the water inflow rate. The model used here refers to very slow water inflow rates ($q_f \leq 0.0001$ L/min) and is not verified.

Pellets properties

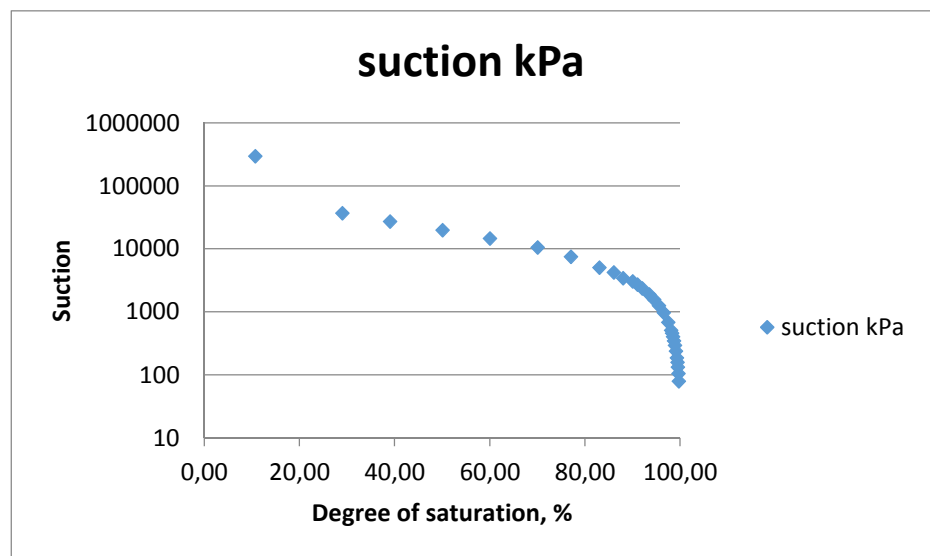
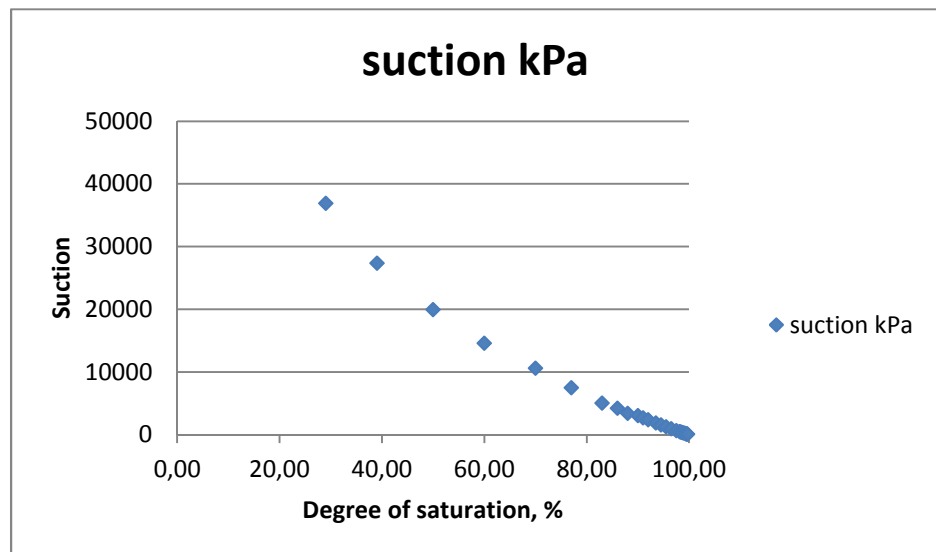
$$e_0 = 1.78$$

Hydraulic

The retention curve is derived from the same relation between the water ratio and suction that is used for the other bentonite parts (see Åkesson et al. 2010a) and shown in Table 4-1.

Table 4-1. Retention curve of the pellet filling.

Sr %	Suction kPa
10.66	295088
29.00	36925
39.00	27366
50.00	19977
60.00	14623
70.00	10616
77.00	7526
83.00	5075
86.00	4230
88.00	3449
90.00	3080
91.00	2724
92.00	2380
93.50	1887
94.50	1571
95.50	1266
96.50	969
97.50	682
98.10	514
98.30	458
98.50	403
98.70	349
98.90	294
99.10	240
99.30	186
99.40	159
99.50	133
99.60	106
99.70	79
100.00	0



Hydraulic conductivity:

$$K = S_r^\alpha \cdot K_0 \quad (4-1)$$

The relation between the hydraulic conductivity and the void ratio is described in Table 4-2. This relation corresponds to the actual hydraulic conductivity of the bentonite and is called the reference model.

Table 4-2. Relation between hydraulic conductivity and void ratio for the pellet filling (reference model).

e	K_θ (low inflow rate) $\alpha=3.0$
1.78	$1.0 \cdot 10^{-12}$
1.60	$2.0 \cdot 10^{-12}$
1.40	$4.0 \cdot 10^{-12}$
1.20	$8.0 \cdot 10^{-13}$
1.00	$2.75 \cdot 10^{-13}$
0.80	$1.0 \cdot 10^{-13}$

Equation 4-1 with $\alpha=3.0$ and the hydraulic conductivity described in Table 4-2 correspond to a standard model of bentonite used for water unsaturated compacted bentonite. A pellet filling is more complicated since there are two types of water transport ways, in the open space between the separate pellets and in the highly compacted separate pellets. This means that the water transport probably behaves in different ways dependant on the inflow rate. At high inflow rate the water can flow freely in the open large pores between the pellets yielding a very high hydraulic conductivity while at very low inflow rate (that is modelled here) water needs to either be transported in the separate pellets (like in highly compacted bentonite) or by diffusion in the pore air between the pellets, which means that the low hydraulic conductivity shown in Table 4-2 probably is relevant. These processes are analysed in Chapter 3.

However, the low density of the pellet filling leads to that there is no resistance to high water pressure. There will be piping if the water pressure exceeds a couple of hundred kPa until the bentonite blocks have swelled so much that the pellet filling has been consolidated to a high density. In order to handle the problem with piping some alternative material models have been tested with high hydraulic conductivity close to water saturation. Table 4-3 shows the models.

Table 4-3. Alternative models for the hydraulic behaviour of pellet filling. Hydraulic conductivity K as function of degree of saturation S_r .

Alternative model 1 $e=1.78$		Alternative model 2 $e=1.78$	
S_r	K	S_r	K
<0.90	Equation 4-1	<0.90	Equation 4-1
0.90	$1.0 \cdot 10^{-12}$	0.90	$1.0 \cdot 10^{-12}$
0.91	$1.0 \cdot 10^{-11}$	0.91	$1.0 \cdot 10^{-10}$
0.92	$1.0 \cdot 10^{-10}$	0.92	$1.0 \cdot 10^{-8}$
0.93	$1.0 \cdot 10^{-9}$	0.93	$1.0 \cdot 10^{-6}$
0.94	$1.0 \cdot 10^{-8}$	0.94	$1.0 \cdot 10^{-4}$
0.95	$1.0 \cdot 10^{-7}$	0.95	$1.0 \cdot 10^{-2}$
0.96	$1.0 \cdot 10^{-6}$	0.96	1.0
1.00	$1.0 \cdot 10^{-6}$	1.00	1.0

The change to high hydraulic conductivity is done in order to simulate that piping will occur when the water pressure in the fracture gets positive and that can only take place when the pellet filling is close to water saturation. The piping will probably stop when the bentonite blocks have compressed the pellet filling to a high density yielding a high swelling pressure.

Mechanical

The mechanical processes are modelled in an identical way as the other bentonite parts but with different parameter values. The models are described in Åkesson et al. (2010a).

Porous elastic

$$\kappa=0.21$$

$$\nu=0.4$$

Moisture swelling

Moisture swelling controls the average total stress to be linear between 0 and 50 kPa between the degree of saturation 29 and 100% as follows:

$$S_r=0.29 \rightarrow \sigma_i=0 \text{ kPa}$$

$$S_r=1.0 \rightarrow \sigma_i=50 \text{ kPa}$$

Initial conditions

$$S_r=0.29$$

$$u=-36925 \text{ kPa}$$

$$\sigma_i=0$$

Contact surfaces

Contact surfaces are applied on all contacts between bentonite materials and their non-bentonite contacts.

$$\phi=8.5^\circ \text{ at all contacts}$$

4.5 Modelling strategy

As shown in Figure 4-1 the inflow takes place in one point in the symmetry plane at the midpoint of the canister. The inflow is modelled in a special way. A constant inflow rate q_f is forced to the inflow point. However, since the water pressure in the rock cannot exceed about 4 MPa that condition is applied. Another factor that is important is that the inflow rate q_f is related to free inflow into the empty deposition hole. If there is a resistance to inflow that creates a water pressure larger than zero at the inflow point the inflow rate will be decreased since the hydraulic gradient over the fracture decreases. The effect of this is not known and not automatically taken into account since the rock is not modelled. Instead a procedure according to Equations 4-2 and 4-3 that reduces the inflow rate proportionally to the pore water pressure at the inflow point is applied.

$$q=q_f(4.0-u_i)/4.0 \quad (4-2)$$

$$q=q_f \text{ if } u_i < 0 \quad (4-3)$$

where

q = water inflow rate
 q_f = water inflow rate at free inflow ($u_i=0$)
 u_i = water pressure at the inflow point

In addition, the flow is thus limited to q_f if the pore pressure in the inflow point is negative.

4.6 Modelling results – constant inflow rate

4.6.1 General

A large number of different calculations has been done with a constant inflow rate modelled according to section 4.5. Convergence problems and questions about the hydraulic behaviour of the pellet filling have dominated the work. Three different types of results will be shown:

1. HM-calculation
2. HM-calculation with fixed nodes in the pellet filled slot
3. H-calculations of only the pellet filled slot

The hydraulic behaviour of the pellet filling has also been considered with different K-values in order to have a wetting behaviour that better reflects the actual behaviour. The two alternative models shown in Table 4-3 have been used and the results compared.

4.6.2 HM-calculation of the entire deposition hole – 0.0001 L/min

The element mesh shown in Figure 4-1 and the material models described in section 4.4 were used for this calculation and the inflow rate was 0.0001 L/min. The reference model of the hydraulic conductivity was used in this calculation i.e. Equation 4-1 and Table 4-2.

It was not possible to run the calculation to full saturation due to convergence problems. The last point of time where results are available is after 10^{10} seconds or 320 years.

Figure 4-2 shows the degree of saturation at different times and Figure 4-3 shows the pore-water pressure at the same times. Figure 4-5 shows the total stress and the void ratio distribution in the symmetry plane after 320 years, while Figure 4-6 shows history plots of the degree of saturation for a number of points in a bentonite ring and the pellet filling.

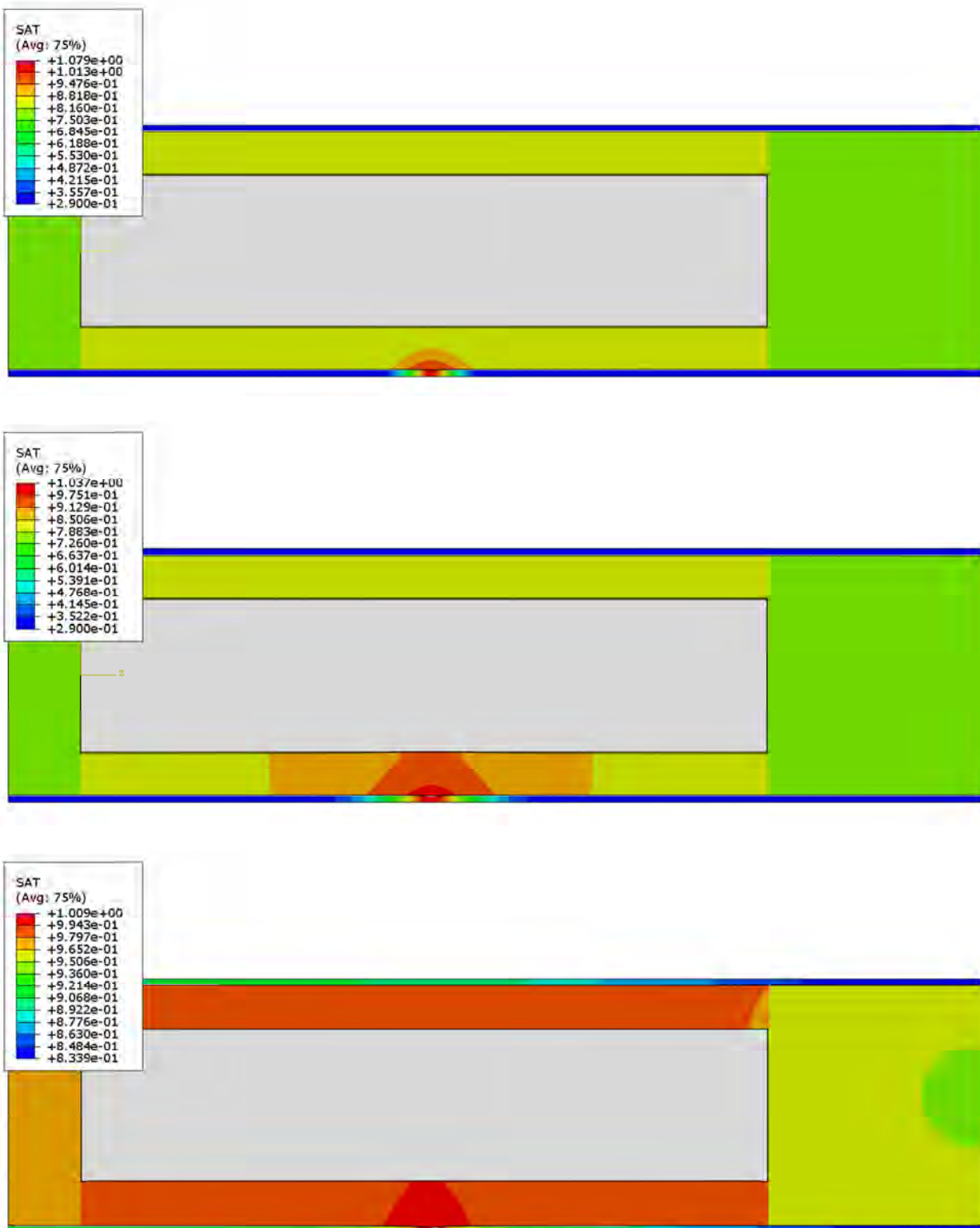


Figure 4-2. HM-modelling of an entire deposition hole with the point inflow rate of 0.0001 L/min. Degree of saturation after 0.32 years (upper), 3.2 years (middle) and 320 years (lower).

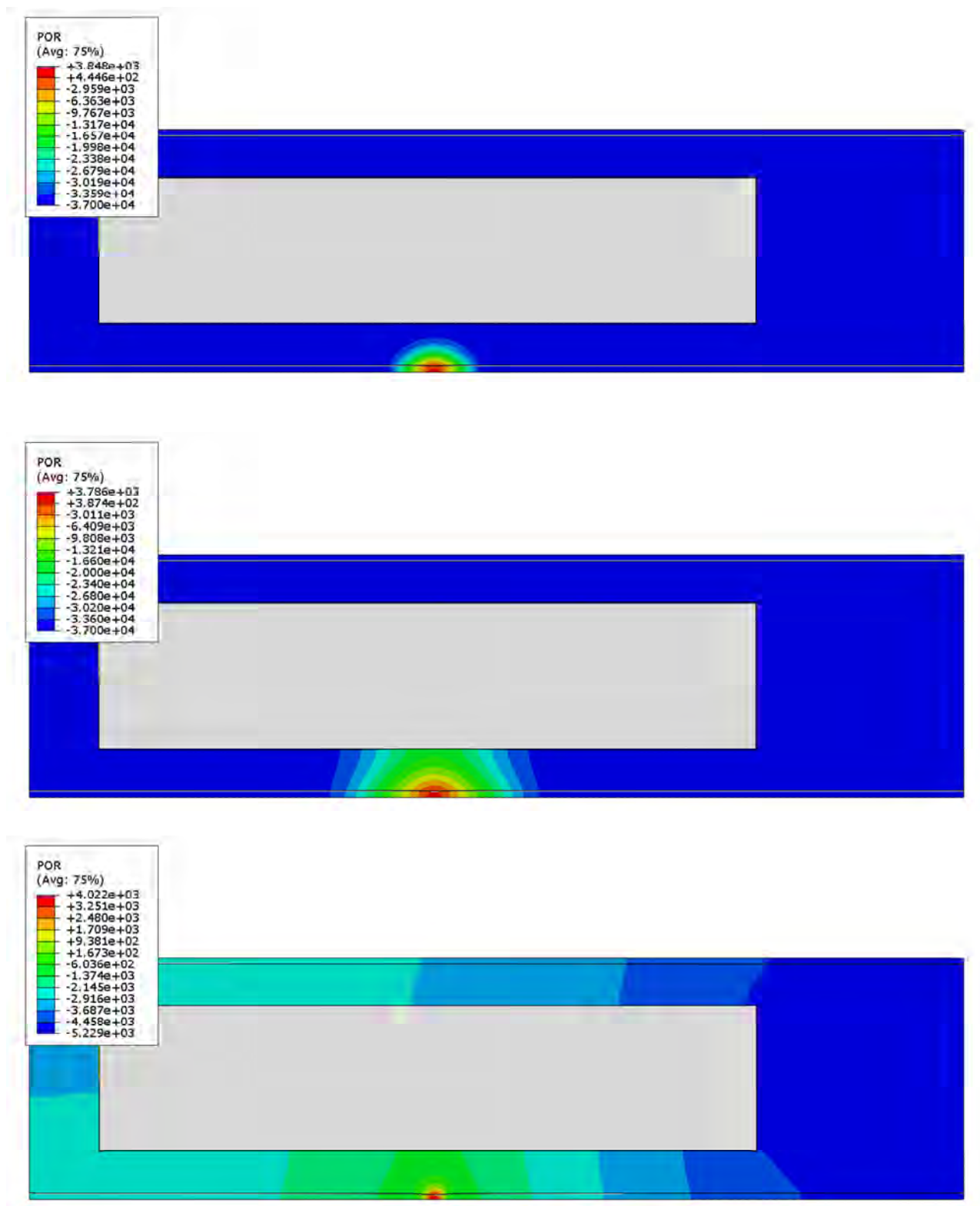


Figure 4-3. HM-modelling of an entire deposition hole with the point inflow rate of 0.0001 L/min. Pore-water pressure (kPa) after 0.32 years (upper), 3.2 years (middle) and 320 years (lower).

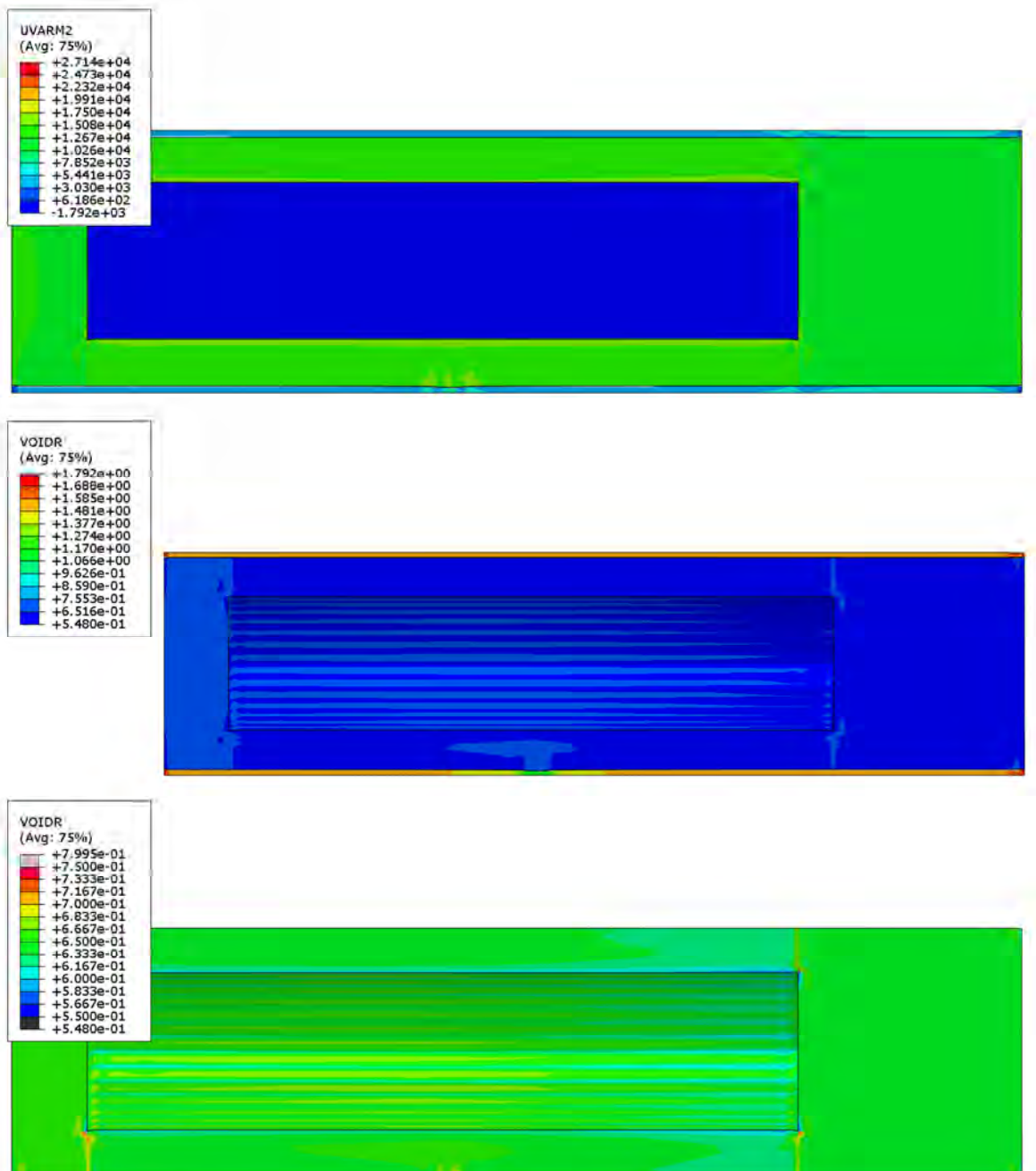


Figure 4-4. HM-modelling of an entire deposition hole with the point inflow rate of 0.0001 L/min. Total stress (kPa) (upper) and void ratio (lower) after 320 years. The lower picture shows the void ratio in the blocks and rings only and at another scale.

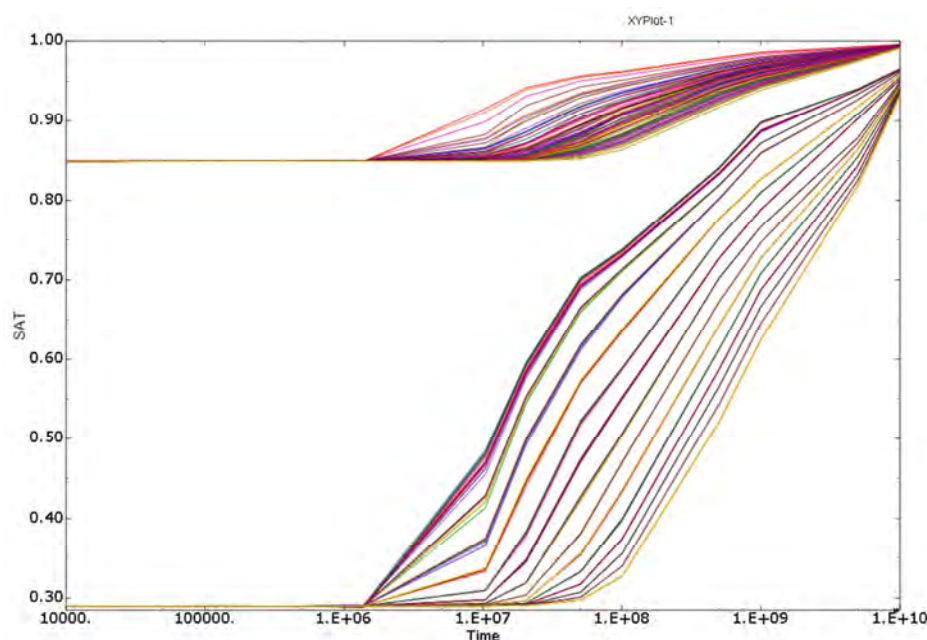


Figure 4-5. HM-modelling of an entire deposition hole with the point inflow rate of 0.0001 L/min. History plots of degree of saturation for different points in the bentonite rings (upper curves) and the pellet filling according to view 1 and view 2 in Figure 4-1.

This model leads to a number of different observations:

After 320 years almost the entire bentonite in the blocks and rings have a degree of saturation larger than 95%, while only a small part of the pellet filling has such a high degree of saturation. The reason for this difference is that the pore-water pressure (suction) is the same in the blocks/rings and the pellet filling in almost all horizontal sections, which yields different degree of saturation due to the difference in density.

There is a large gradient in pore-water pressure in the pellet filled slot during the entire saturation period since the water transport rate in the pellets is slow compared to the inflow rate.

The pore-water pressure is very high in the inflow point during the entire period, which yields a choking of the inflow rate according to Equation 4-1. The water pressure is much higher than the pellet filling can be expected to withstand.

Extrapolation of the history curves leads to an estimated time to full saturation of about 1500 years. This is about 50 times longer than the time it would take to saturate the buffer meaning that the average inflow rate is only about $2 \cdot 10^{-6}$ L/min instead of 10^{-4} L/min.

The inflow rate is thus much lower than the intended inflow rate due to the choking of the inflow. The results are thus probably not representative for the inflow rate 10^{-4} L/min but may be used to study the homogenisation at an inflow rate of about $2 \cdot 10^{-6}$ L/min if the pellet filling is not able to prevent water inflow by piping. The degree of saturation and the pore-water pressure plots (Figures 4-2 and 4-3) show that in the beginning after 3.2 years the wetting is very uneven, but after long time (320 years) the wetting has been more evenly distributed and takes place from the entire pellet filling although there are still large gradients in the pellet filling. The void ratio distribution after 320 years, when the degree of saturation in almost all the high density part (blocks and rings) is more than 95%, is not very inhomogeneous as shown in Figure 4-4. The influence is very local around the inflow point with lower void ratio in the pellet filling and higher in the neighbouring parts of the bentonite rings. It should though be noted that the simulation was not run to complete water saturation.

4.6.3 HM-calculation of the entire deposition hole with fixed nodes of the pellet filled slot – inflow 0.0001 l/min

Since the calculation in the previous section was not completed due to convergence problems a new model, identical to the previous one but with all nodes of the pellet filling fixed, was made. The problems of convergence, which are often related to deformed elements, could in this way be overcome.

The same history curves of degree of saturation as shown in Figure 4-5 are shown for the fixed nodes calculation in Figure 4-6. The figure shows that the buffer is saturated after $5 \cdot 10^{10}$ seconds corresponding to 1 585 years, which was also concluded for the calculation without fixed nodes.

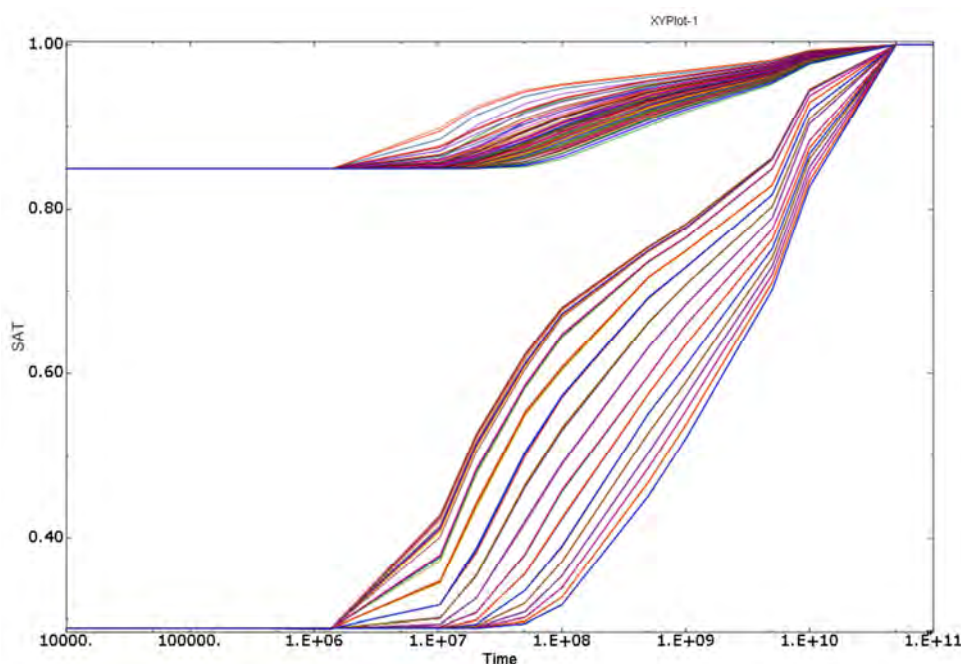


Figure 4-6. HM-modelling of an entire deposition hole with the point inflow rate of 0.0001 L/min in the model with fixed nodes of the pellet filling. History plots of degree of saturation for different points in the bentonite rings and the pellet filling.

4.6.4 H-calculations of only the pellet filled slot

In order to study the flow behaviour in a pellet-filled slot a number of calculations have been done with the rest of the model excluded. Results from the models described in Table 4-4 will be shown:

Table 4-4. Calculations with pellets filled slot only.

Model	See Table	Inflow rate	Remark
Reference model	4-2	10^{-4} L/min	
Alternative model 1	4-3	10^{-4} L/min	Increased K at $S_r > 90\%$; $K_{max} = 10^{-6}$ m/s
Alternative model 2	4-3	10^{-4} L/min	Increased K at $S_r > 90\%$; $K_{max} = 1$ m/s
Alternative model 2	4-3	10^{-6} L/min	Increased K at $S_r > 90\%$; $K_{max} = 1$ m/s

Figures 4-7, 4-8, 4-9 and 4-10 illustrate the results and the differences for the calculations with the inflow rate 10^{-4} L/min. The results from all three models are shown and compared in each figure.

The pore pressure distribution after 3.2 years and 32 years are shown in Figures 4-7 and 4-8. The degree of saturation after 32 years is shown in Figure 4-9. In Figure 4-10 the calculated total inflow is plotted as function of time.

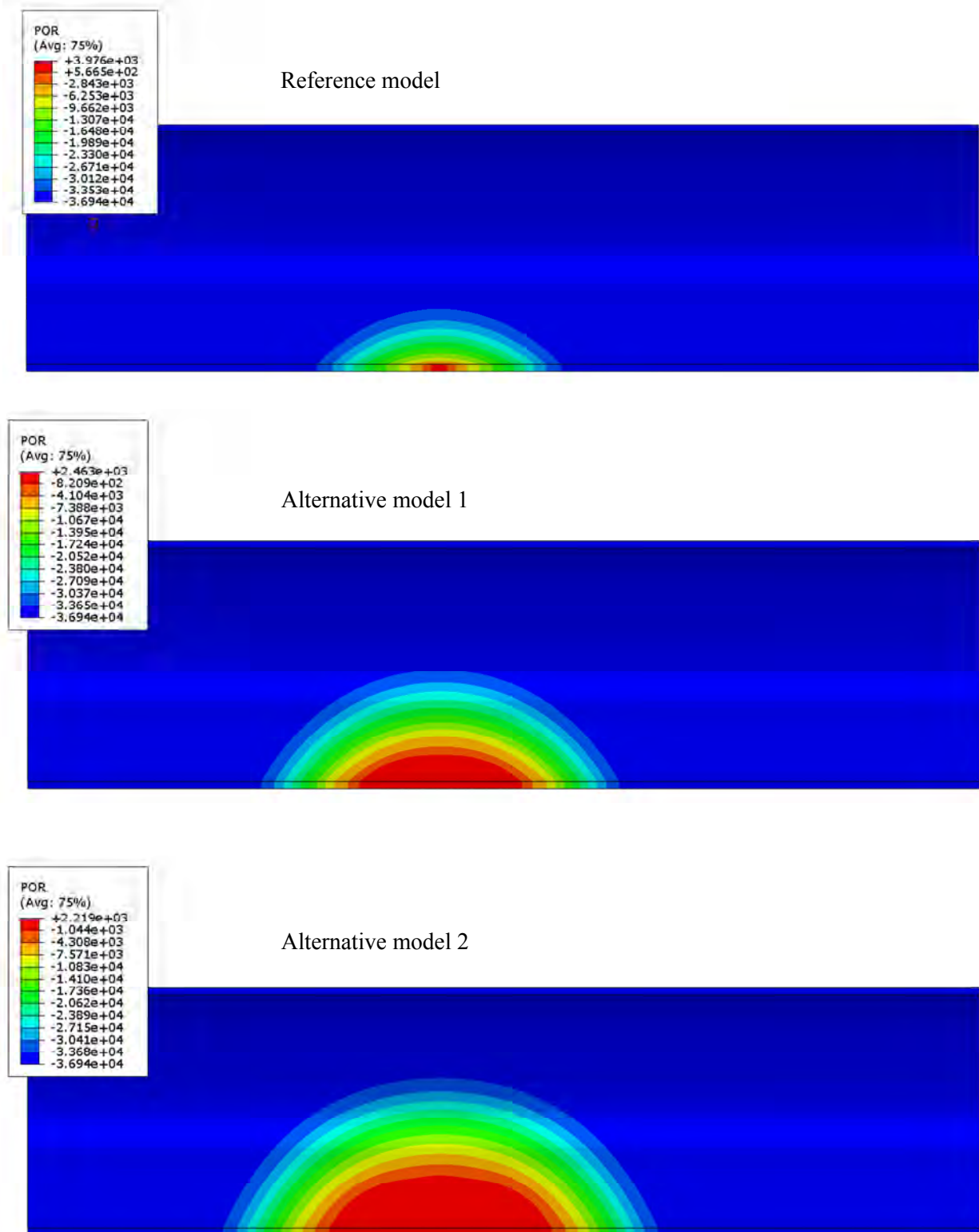


Figure 4-7. H-modelling of pellet filled slot only with the point inflow rate of 0.0001 L/min. Pore-water pressure (kPa) after 3.2 years.

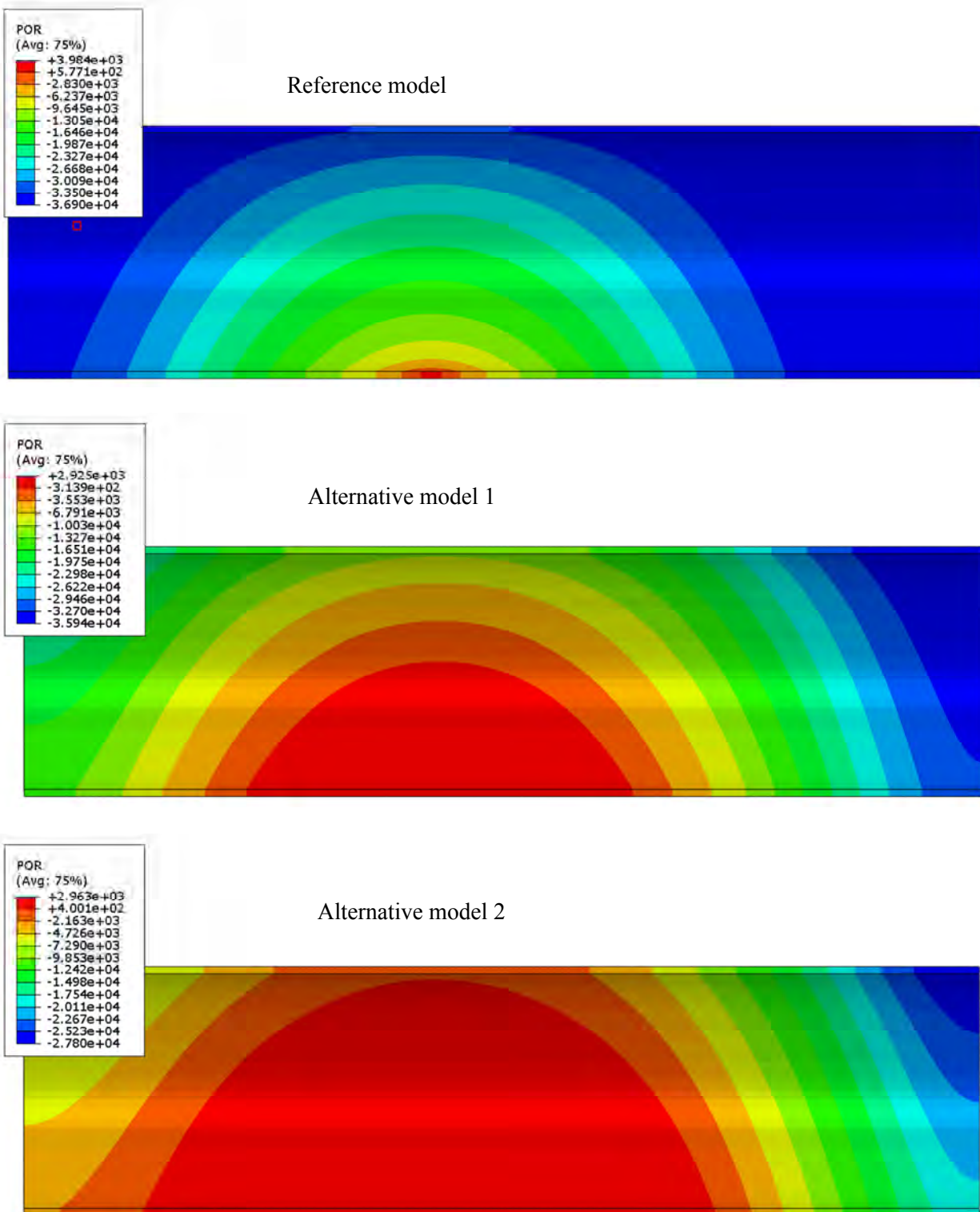


Figure 4-8. H-modelling of pellet filled slot only with the point inflow rate of 0.0001 L/min. Pore-water pressure (kPa) after 32 years.

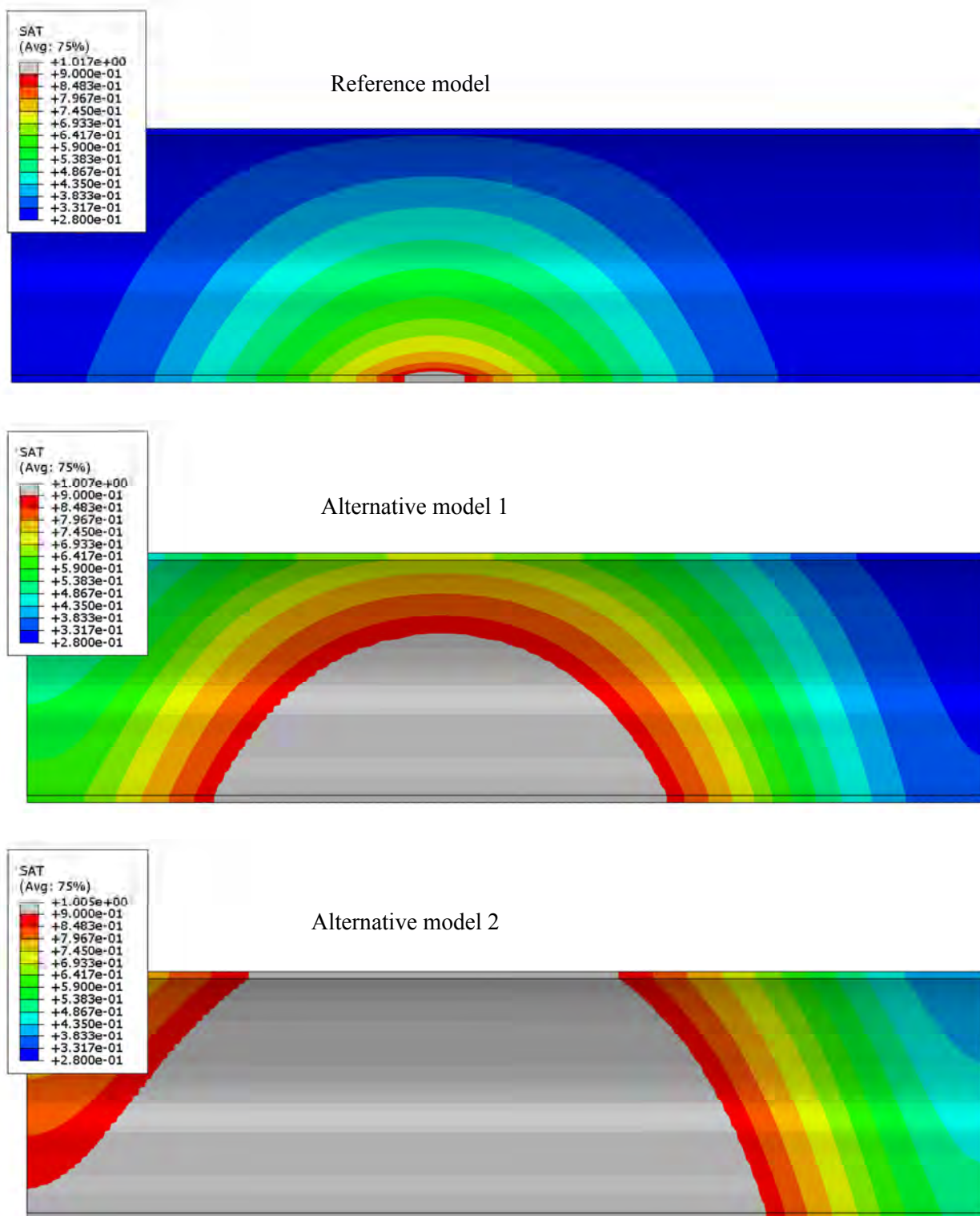


Figure 4-9. H-modelling of pellet filled slot only with the point inflow rate of 0.0001 L/min. Degree of saturation after 32 years.

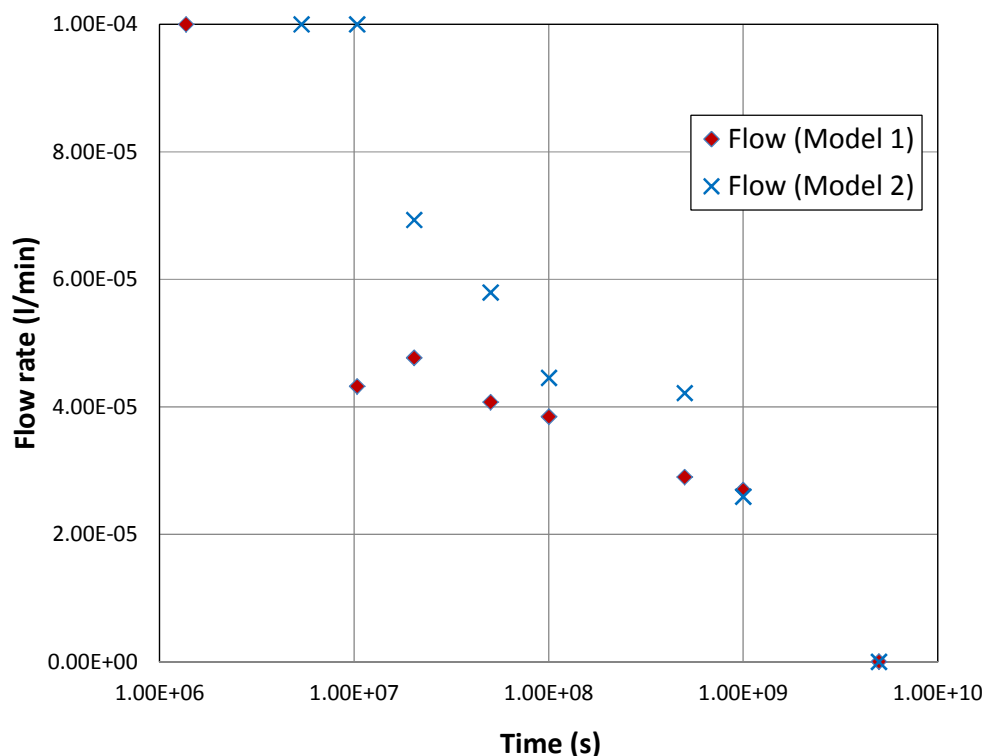


Figure 4-10. Inflow rate as function of time for alternative models 1 and 2.

The attempts to better model the inflow distribution with the alternative models yields some obvious results. The pore pressure at the inflow point is reduced but still too high. The propagation of the pore water into the pellet filled slot is faster. The time to full saturation is about $5 \cdot 10^9$ seconds (≈ 150 years) for the alternative models and 10 times longer for the reference model. It is, however, still 10 times longer than the theoretical time to fill up the slot if the inflow rate was constant 0.0001 L/min, which means that the actual average inflow rate in the alternative models is 10 times lower. There is also some difference between the alternative models with faster wetting in model 2 due to the higher hydraulic conductivity adapted at $S_r > 90\%$.

The results from the calculation with the inflow rate 10^{-6} L/min are shown in Figures 4-11 to 4-13. Figure 4-11 shows the pore-water pressure at three different times, Figure 4-12 shows the degree of saturation at the same times and Figure 4-14 shows the inflow rate and the pore pressure in the inflow points as function of time.

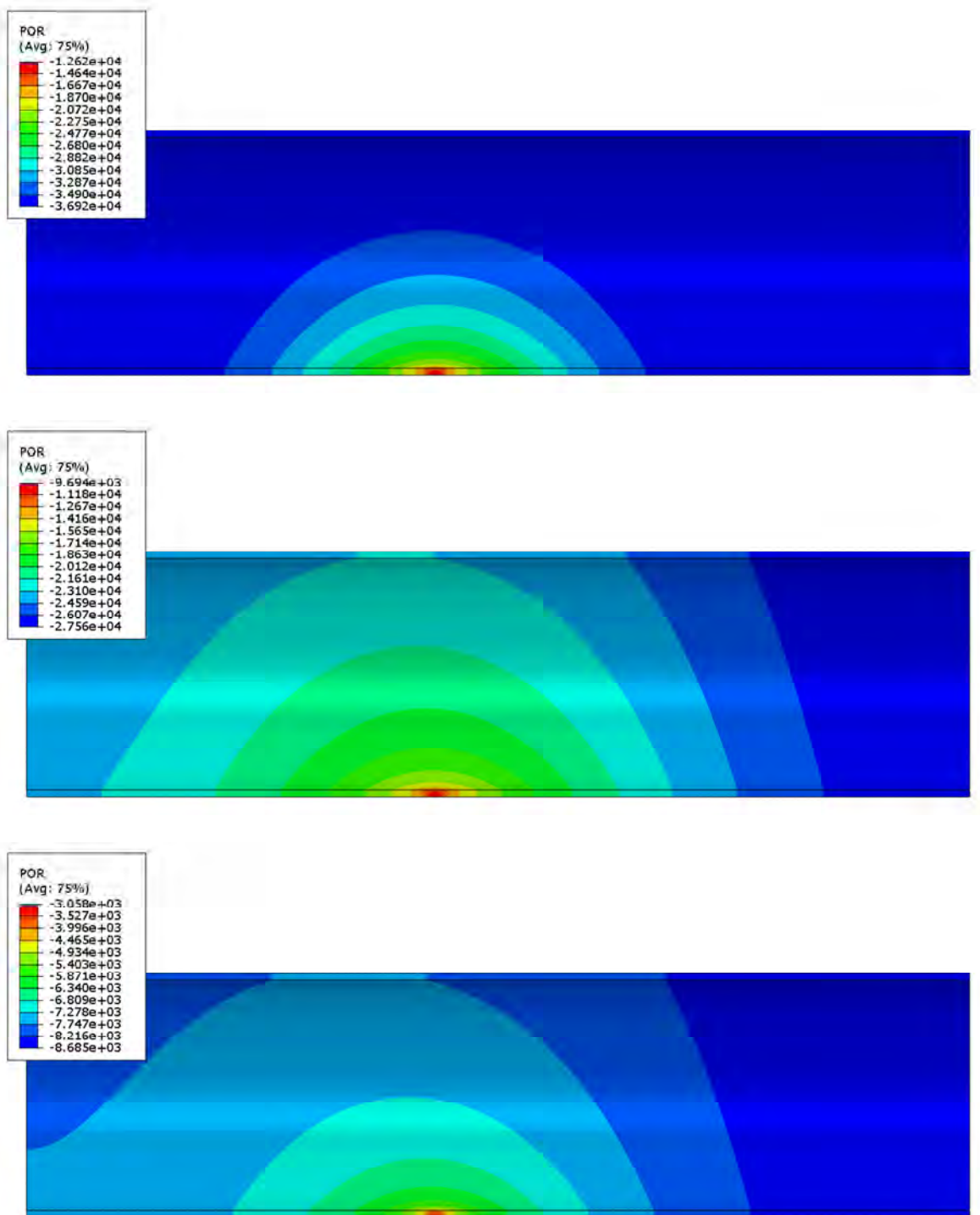


Figure 4-11. H-modelling of pellet filled slot only with the point inflow rate of 10^{-6} L/min. Pore-water pressure (kPa) after 32 years, 320 years and 950 years.

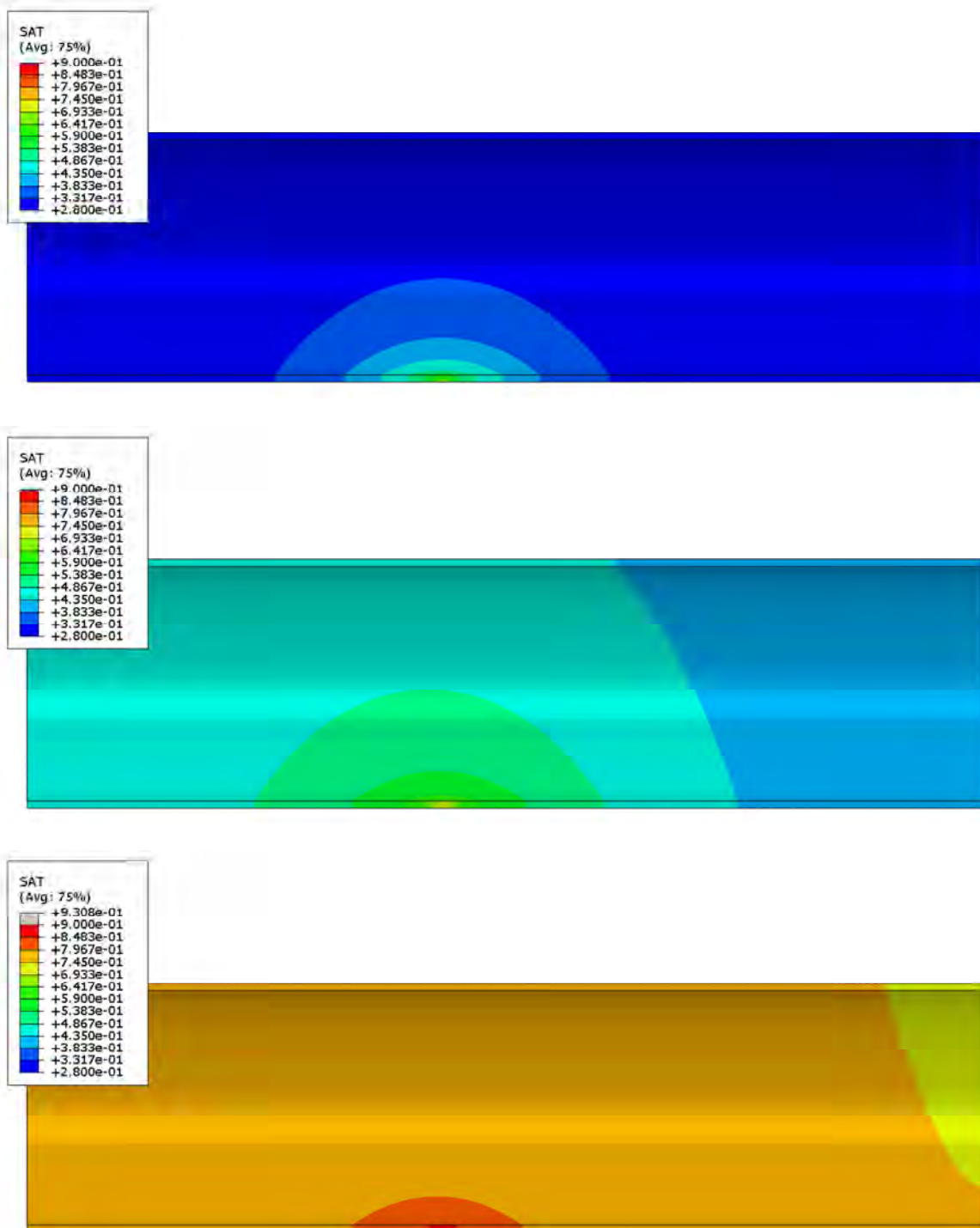


Figure 4-12. H-modelling of pellet filled slot only with the point inflow rate of 10^6 L/min. Degree of saturation after 32 years, 320 years and 950 years.

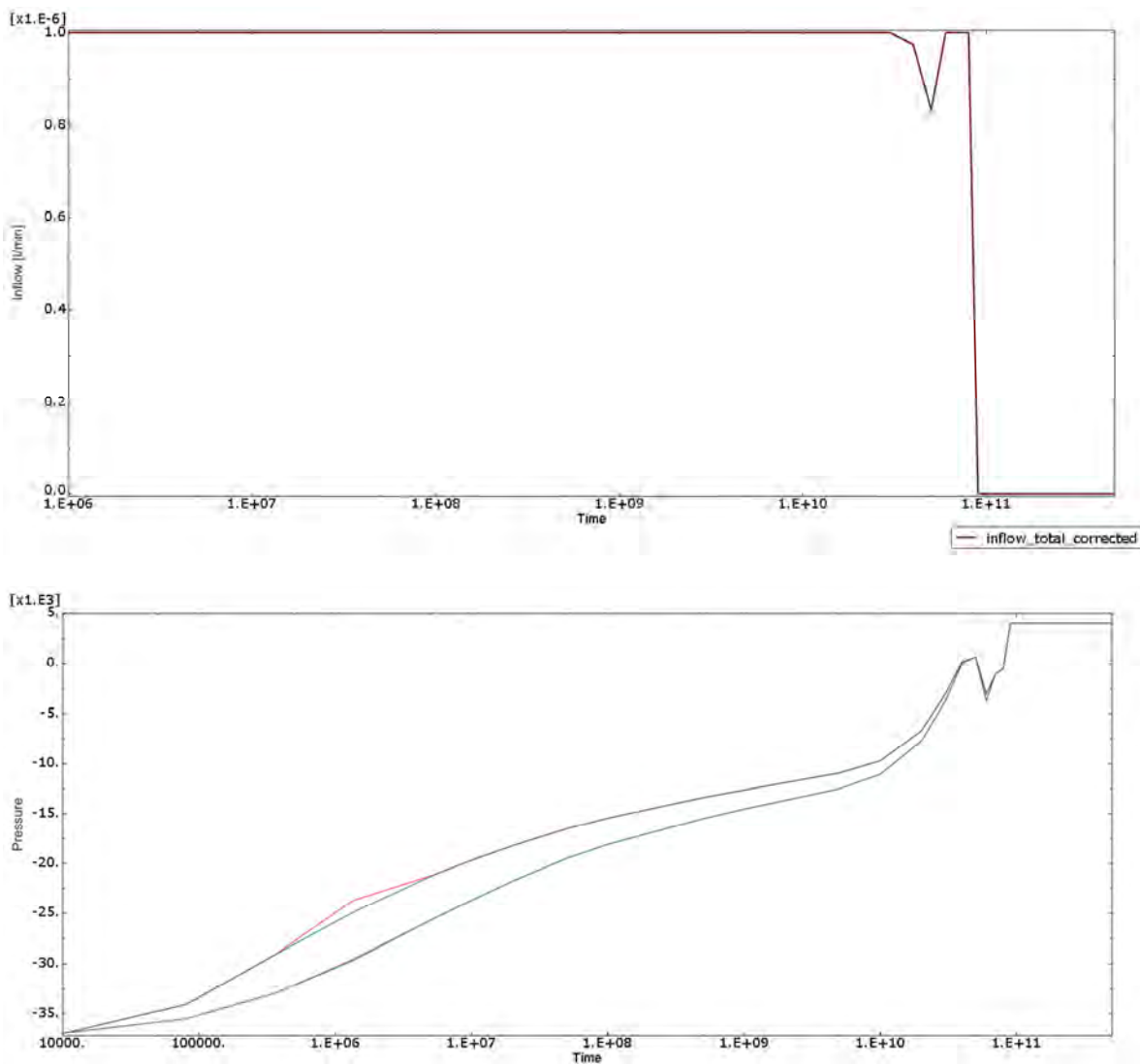


Figure 4-13. H-modelling of pellet filled slot only with the point inflow rate of 10^{-6} L/min. Total inflow (upper) and pore pressure (kPa) in the inflow points as function of time (s).

The figures show that the wetting is rather slow. The pore pressure in the inflow points is always negative meaning that the pellet filling can take more water than the inflow. The inflow rate is constant during almost the entire calculation since it has been set at 10^{-6} L/min according to the condition in Equation 4-3. After $3 \cdot 10^{10}$ seconds (950 years), the inflow is reduced since the pore pressure gets positive. Some strange irregularities occur after that time but the inflow decreases and full saturation is reached after 1500 – 2000 years whereupon the pore pressure is 4 MPa and the inflow zero.

4.7 Modelling results – constant water pressure

4.7.1 General

Four simulations with constant water pressure were also run. In two of them the inflow was located in one point as the simulations shown in Sections 4.4-4.6. In the other two the flow was instead located as a line source. Since there were large problems with convergence each simulation were also at first run with fixed nodes in the pellet filling. Unfortunately only the point inflow simulations yielded results that can be used.

4.7.2 Point inflow and fixed nodes of the pellet filling

This simulation was identical to the one shown in Section 4.6.3, with the only difference that a constant inflow rate was changed to constant water pressure $u=0$ kPa.

Figure 4-14 shows history plots of the pore-water pressure in a number of points in the pellets and the bentonite rings. Figure 4-15 shows the water inflow rate as function of time and Figures 4-16 and 4-17 show the pore-water pressure and the degree of saturation after 320 years and 3200 years.

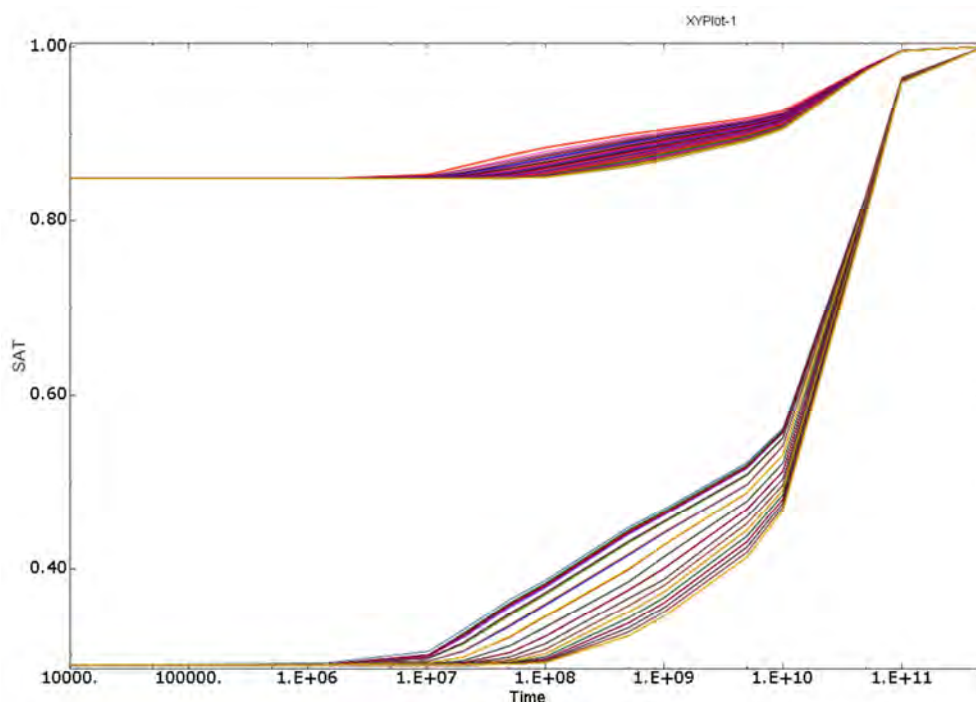


Figure 4-14. HM-modelling of an entire deposition hole with point inflow and constant pore-water pressure in the model with fixed nodes of the pellet filling. History plots of degree of saturation for different points in the bentonite rings and the pellet filling.

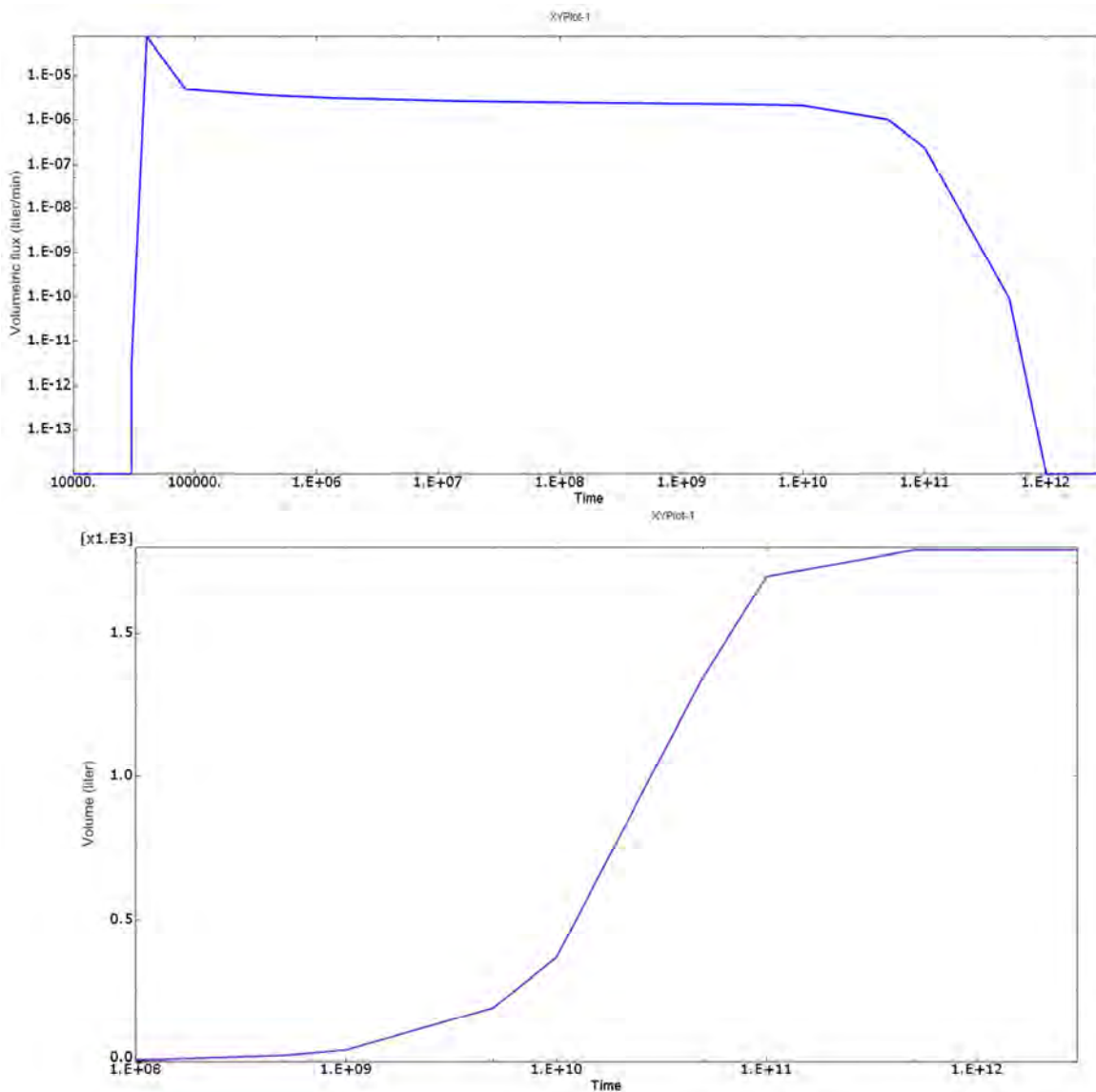


Figure 4-15. HM-modelling of an entire deposition hole with point inflow and constant pore-water pressure in the model with fixed nodes of the pellet filling. Water inflow rate (upper) and total water inflow as a function of time (s).

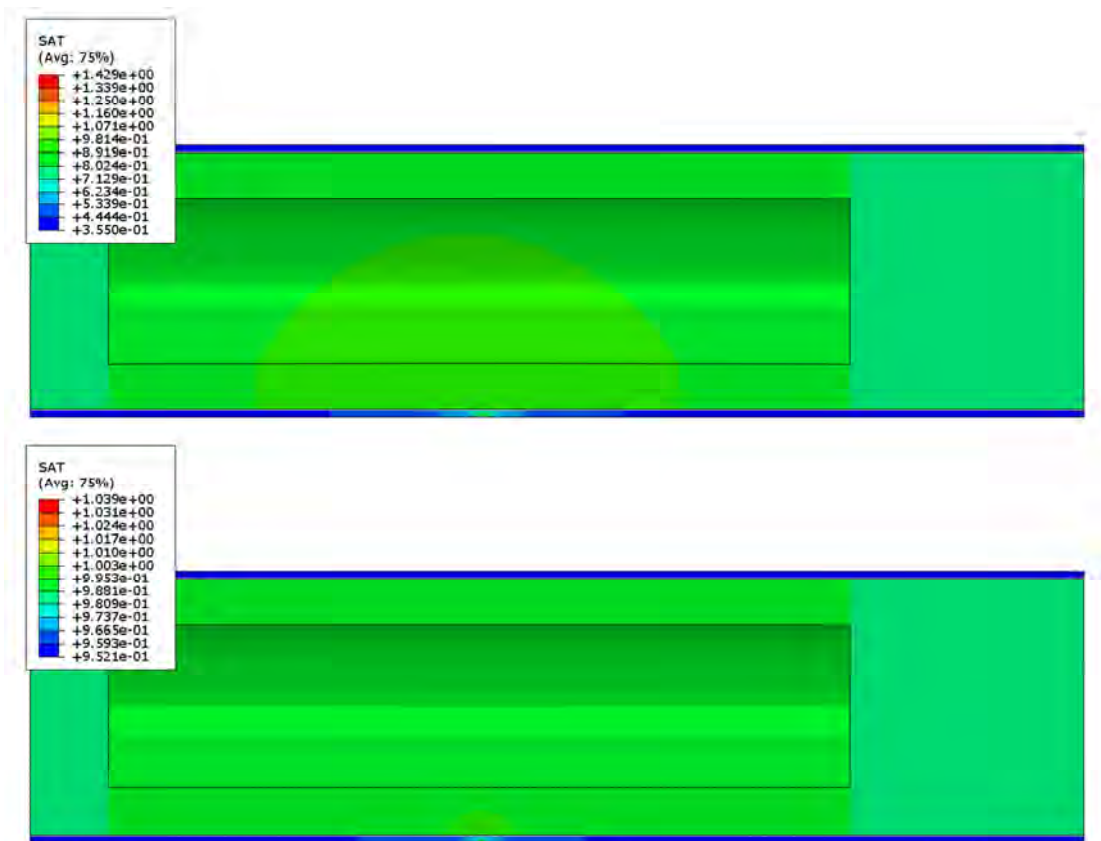


Figure 4-16. HM-modelling of an entire deposition hole with point inflow and constant pore-water pressure in the model with fixed nodes of the pellet filling. Degree of saturation after 320 years (upper) and 3200 years (lower).

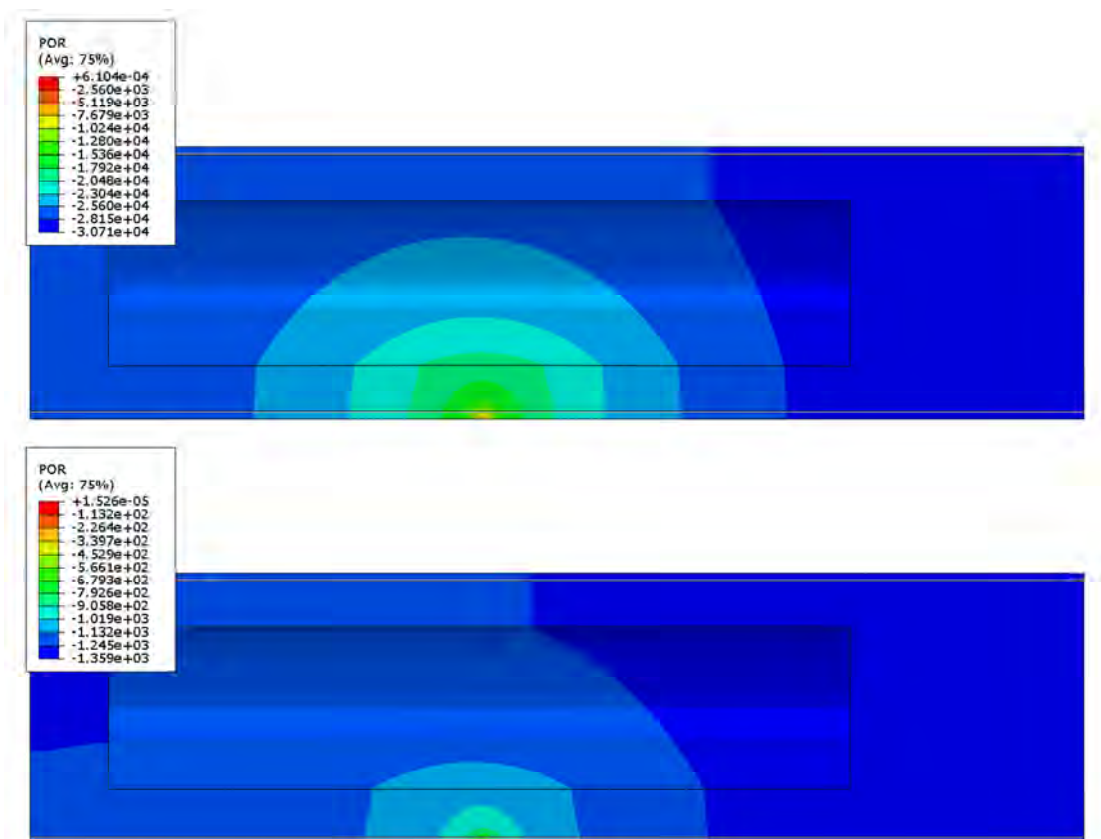


Figure 4-17. HM-modelling of an entire deposition hole with point inflow and constant pore water pressure in the model with fixed nodes of the pellet filling. Pore-water pressure (kPa) after 320 years (upper) and 3,200 years.

The results show that the entire buffer is water saturated after between about 5,000 years and 15,000 years ($1.5 \cdot 10^{11}$ – $4.5 \cdot 10^{11}$ seconds). The water inflow rate is between 10^{-5} and 10^{-6} L/min up until about 1 500 years ($5 \cdot 10^{10}$ s) where after it decreases rapidly.

The wetting is rather inhomogeneous in the beginning, with large gradients in pore-water pressure in the pellet filling after 320 years with still very high suction of 30,000 kPa in large parts. With time the wetting gets more homogeneous and after 3,200 years the pore-water pressure gradient is reduced to about 4% of the original (highest suction about 1,350 kPa).

4.7.3 Point inflow and free nodes of the pellet filling

Because of convergence problems, only results up to about 1,600 years are available. The results are similar to the results of the simulation with fixed pellet nodes, with exception of the void ratio distribution. Figure 4-18 and 4-19 show some contour plots of the situation after 1,600 years.

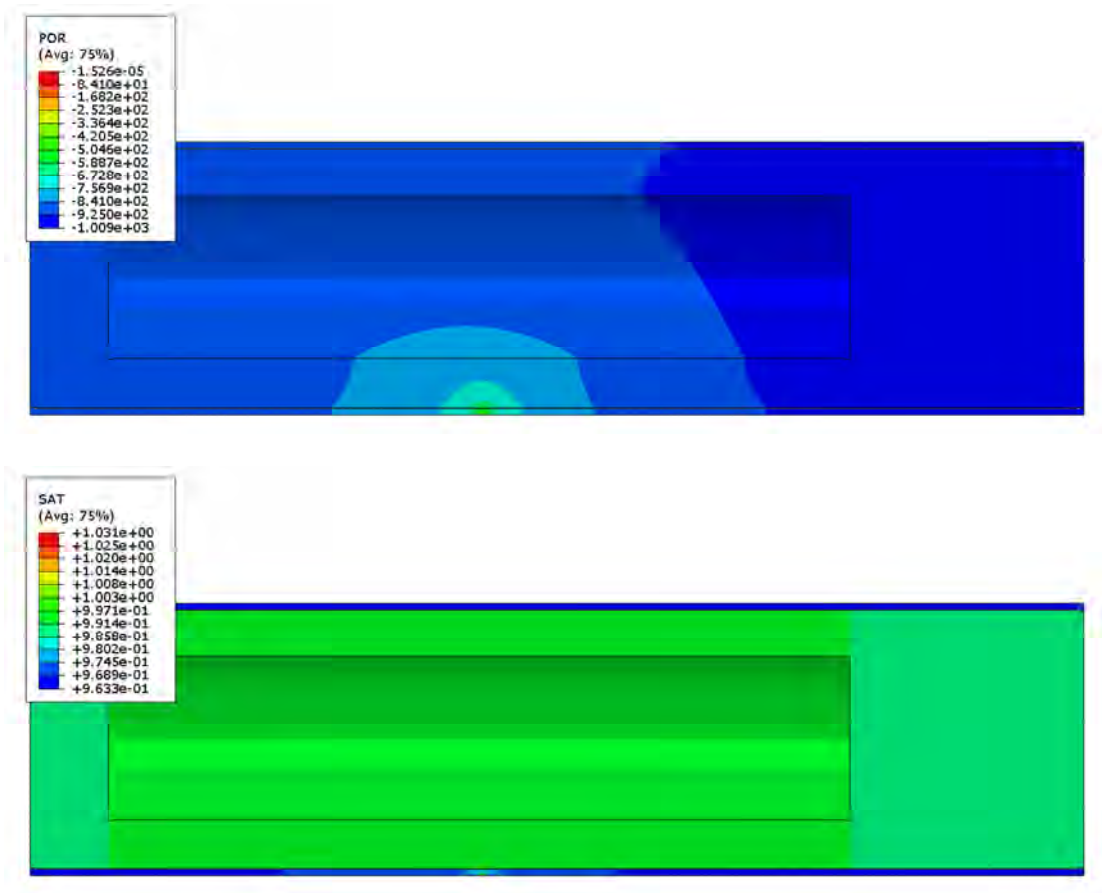


Figure 4-18. HM-modelling of an entire deposition hole with point inflow and constant pore-water pressure in the model with free nodes of the pellet filling. Pore-water pressure (kPa) and degree of saturation after 1,600 years.

Figure 4-18 shows that the pore-water equilibrium has gone rather far and that the degree of saturation is everywhere higher than 96%. In spite of that the simulation is not completed the results can be used to some extent.

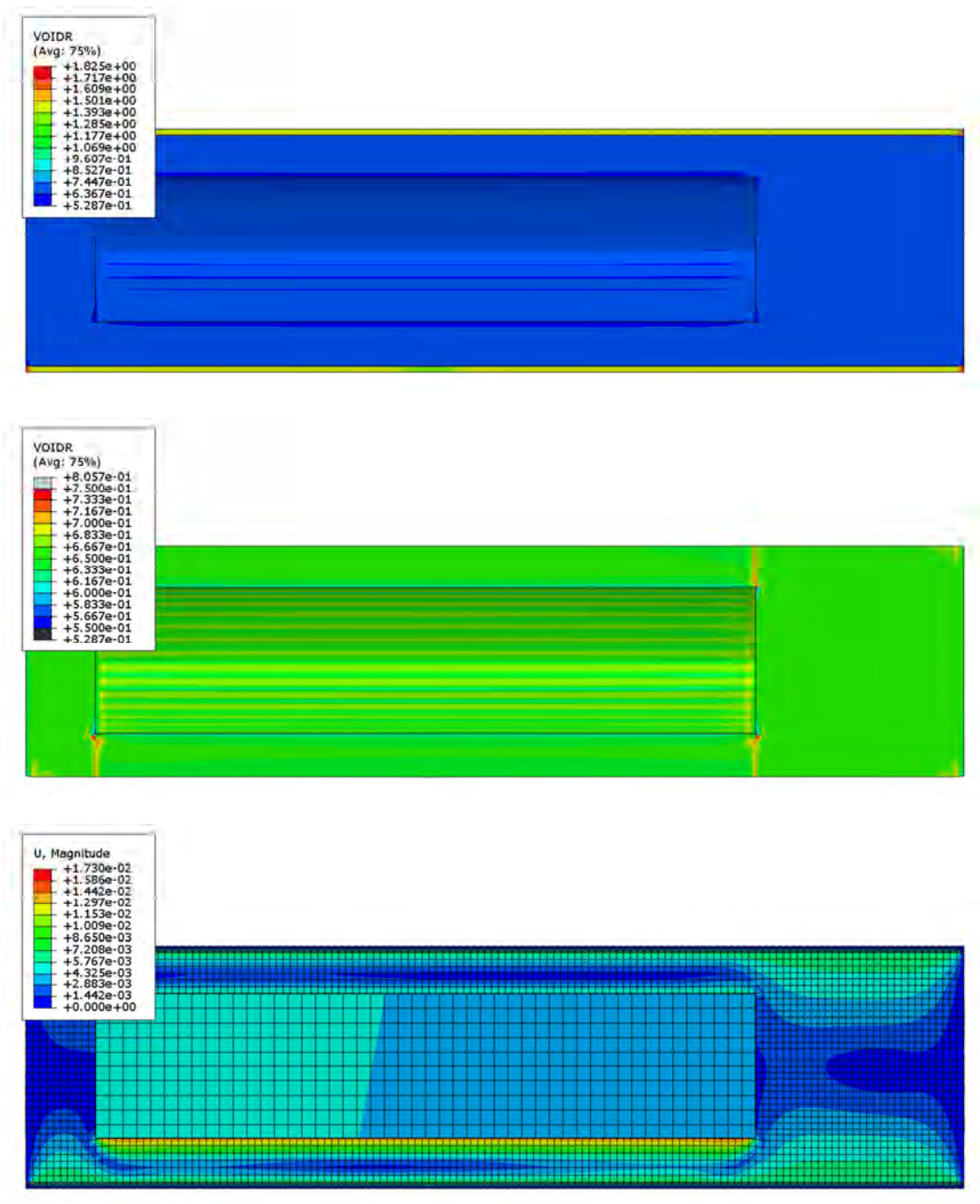


Figure 4-19. HM-modelling of an entire deposition hole with point inflow and constant pore-water pressure in the model with free nodes of the pellet filling. Void ratio of the entire buffer (upper), void ratio of the blocks and rings (middle) and displacements after 1600 years (lower).

Figure 4-19 shows the mechanical consequences with the void ratio distribution and the total displacements. The results show that there is no strong inhomogeneity except from the large difference in void ratio of the block/ring parts and the pellet part, which indicate that the pellet filling is too stiff. The displacement plot shows that the canister has moved about 4 mm away from the water inlet side due to the inhomogeneous wetting.

5. Risks and consequences

In spite of problems with convergence and uncertainties of how water inflow into a pellet filling can be modelled, an analysis of the risks and consequences can be done.

Since uneven wetting will only occur when the inflowing water mainly comes in local spots, the contribution from the rock matrix must be small otherwise there will be a simultaneous homogeneous wetting. As concluded in section 2.1 the matrix hydraulic conductivity is in the range between 10^{-12} m/s and 10^{-13} m/s. If the lower value is used the time to complete water saturation from the rock matrix alone will be about 1,500 years according to the analyses referred to in section 2.2. This means that if a point inflow rate yields a longer time to full saturation of the buffer than about 1,500 years there will be no uneven wetting of the buffer.

According to the volume calculations shown in section 2.3 the time to fill up all empty pores in the buffer is 3,500 years at the point inflow rate 10^{-6} L/min and 350 years at the point inflow rate 10^{-5} L/min. The conclusion is thus that there will only be uneven wetting of the buffer if the point inflow rate is higher than between 10^{-5} L/min and 10^{-6} L/min or about $5 \cdot 10^{-6}$ L/min.

On the other hand, if the point inflow rate is so high that the pellet filling is water filled before the buffer rings have been water saturated close to the inflow point, there will not be an uneven wetting either. As shown in Table 2-2 it will take 1.55 years to fill up the pellet voids at the inflow rate 10^{-3} L/min. The time to saturate the bentonite rings if water is freely available in the pellet filling is about 2 years (Åkesson et al. 2010a). This means that if the inflow rate is higher than 10^{-3} L/min, there will not be an uneven wetting since the pellet filling will be filled and give even wetting in the entire buffer. The requirement for this conclusion is that the water filling of the pellets are equally distributed. This is the case when the inflow rate is lower than 10^{-3} L/min - 10^{-4} L/min as shown in Figure 2-2. For 10^{-3} L/min, the water will seek its way upwards and form a wetting path with water available along a vertical line as shown in Figure 2-2.

The conclusion is thus that uneven wetting can only take place for the following cases:

1. At an inflow rate of about 10^{-3} L/min when water is freely available along a vertical line in the rock surface
2. At inflow rates (into an open deposition hole) between about $5 \cdot 10^{-4}$ L/min - $5 \cdot 10^{-6}$ L/min when water is available at a point in the rock surface

According to Joyce et al. (2013), the number of holes with an expected inflow rate between $5 \cdot 10^{-6}$ L/min and 10^{-3} L/min is about 500 out of 6,916 i.e. every 14:th deposition hole may have uneven wetting.

The simulations yield that a water inflow rate of 10^{-5} L/min - 10^{-6} L/min can be taken by the pellet filling without yielding a high water pressure or a high suction at the inflow point. If the inflow rate is higher, the absence of capability to model piping will cause water pressure in the numerical simulation so high that the inflow cannot be taken by the pellet filling. The calculations that either prescribe or yield water inflow rate of between 10^{-5} L/min and 10^{-6} L/min are thus probably relevant.

The first case above corresponds to the calculation with line inflow. Unfortunately this simulation did not lead to any results. The second case corresponds mainly to the calculations shown in section 4.6.2 with water pressure dependant inflow rate and to the point inflow calculation with constant water pressure shown in Section 4.7. Both these latter calculations have an effective inflow rate of between 10^{-5} L/min and 10^{-6} L/min.

The results of the mechanical simulations of these cases indicate that the inhomogeneity of the buffer caused by the uneven wetting is rather small, although some horizontal displacement of the canister can be expected as well as some local inhomogeneity around the inflow point.

The overall conclusion is thus that the inhomogeneous wetting will not take place in dry holes but in a spectrum of holes (about 500) that have an inflow rate of between $5 \cdot 10^{-6}$ L/min and 10^{-3} L/min and that the influence on the density distribution of the buffer and thus also the swelling pressure on the canister is very limited.

It must though be pointed out that there are several uncertainties about the simulations and analyses made and the main ones being the following two:

The mechanical model of the dry pellet filling in the simulations is not verified and calibrated and it turned out to be a little stiffer than what can be expected after full saturation, which thus underestimates the displacements. However, making it softer would make the convergence more difficult.

The hydraulic model of the dry pellet filling has been made with a number of assumptions that have not been verified. The theoretical analysis (Chapter 3) and the numerical model (Chapter 4) yield similar results but need to be investigated and verified in laboratory tests.

References

- Carslaw H S, Jaeger J C, 1959.** Conduction of heat in solids. 2nd ed. Oxford: Clarendon.
- Dueck A, 2007.** Results from suction controlled laboratory tests on unsaturated bentonite – verification of a model. Experimental Unsaturated Soil Mechanics, Springer Proceeding in Physics 112, 329–335.
- Joyce S, Swan D, Hartley L, 2013.** Calculation of open repository inflows for Forsmark. SKB R-13-21, Svensk Kärnbränslehantering AB.
- SKB 2010.** Buffer production report, Design, production and initial state of the buffer. SKB TR-10-15, Svensk Kärnbränslehantering AB.
- Svensson U, Follin S, 2010.** Groundwater flow modelling of the excavation and operational phases – Forsmark. SKB R-09-19, Svensk Kärnbränslehantering AB.
- Vilks P, 2007.** Forsmark site investigation. Rock matrix permeability measurements on core samples from borehole KFM01D. SKB P-07-162, Svensk Kärnbränslehantering AB.
- Åkesson M, 2013.** 1.4. Bentonites other than MX-80. Clay Technology. SKBdoc 1415875, ver 1.0, Svensk Kärnbränslehantering AB.
- Åkesson M, Kristensson O, Börgesson L, Dueck A, Hernelind J, 2010a.** THM modelling of buffer, backfill and other system components. Critical processes and scenarios. SKB TR-10-11, Svensk Kärnbränslehantering AB.
- Åkesson M, Börgesson L, Kristensson O, 2010b.** SR-Site Data report. THM modelling of buffer, backfill and other system components. SKB TR-10-44, Svensk Kärnbränslehantering AB.